ISSN 2427-4577

BULLETIN N° 242
ACADÉMIE EUROPEENNE INTERDISCIPLINAIRE DES SCIENCES
INTERDISCIPLINARY EUROPEAN ACADEMY OF SCIENCES

Lundi 3 février 2020 à 16h30
à l'Institut Curie, Amphi BURG salle annexe 2
12, rue Lhomond 75005 PARIS

16h30: examen de candidatures
17h:Conférence:
« Des circuits électriques quantiques »
par Daniel ESTÈVE
Directeur de Recherche au CEA
Membre de l'Académie des Sciences
Quantronique, Service de Physique de l'Etat Condensé, CEA-Saclay

Notre Prochaine séance aura lieu le lundi 2 mars 2020 à 17h
à l'Institut Curie, Amphi BURG salle annexe 2
12, rue Lhomond 75005 PARIS

Elle aura pour thème

Conférence:
« Des systèmes et matériaux (ré)actifs chez les plantes»
par Olivier HAMANT
Directeur de Recherche à l'INRA
Laboratoire de reproduction et développement des Plantes /ENS Lyon

ACADÉMIE EUROPÉENNE INTERDISCIPLINAIRE DES SCIENCES
INTERDISCIPLINARY EUROPEAN ACADEMY OF SCIENCES

février 2020
N°242

TABLE DES MATIERES

Prochaine séance : lundi 2 mars 2020

Conférence:

« Des systèmes et matériaux (ré)actifs chez les plantes»

par Olivier HAMANT
Directeur de Recherche à l'INRA
Laboratoire de reproduction et développement des Plantes /ENS Lyon

ACADEMIE EUROPEENNE INTERDISCIPLINAIRE DES SCIENCES
Fondation de la Maison des Sciences de l'Homme, Paris.

Séance du Lundi 3 février/Institut Curie 17h

La séance est ouverte à 16h30 **sous la Présidence de Victor MASTRANGELO** et en la présence de nos Collègues Gilbert BELAUBRE(?), Jean BERBINAU, Jean-Louis BOBIN, Eric CHENIN, Françoise DUTHEIL, Claude ELBAZ, Jean -Pierre FRANCOISE, Michel GONDRAN, Irène HERPE-LITWIN, Claude MAURY, Marie-Françoise PASSINI, Edith PERRIER, Jacques PRINTZ, Alain STAHL , Jean SCHMETS, Jean-Pierre TREUIL.

Etaient également présents nos collègues, membres correspondants Dominique PRAPOTNITCH et Benoît PRIEUR et , en tant que visiteuse Lise BANKIR, Directeur de Recherche émérite à l'INSERM.

Etaient excusés :François BEGON, Jean-Pierre BESSIS, Bruno BLONDEL, Michel CABANAC, Alain CARDON, Juan-Carlos CHACHQUES, Gilles COHEN-TANNOUDJI, Alain CORDIER , Daniel COURGEAU, Sylvie DERENNE, Ernesto DI MAURO, Jean-Félix DURASTANTI, Vincent FLEURY, Robert FRANCK, Dominique LAMBERT, Pierre MARCHAIS, Anastassios METAXAS, Jacques NIO, Pierre PESQUIES, Denise PUMAIN, René PUMAIN, Michel SPIRO,.

I. Examen de Candidatures

Candidature Christian GORINI en tant que membre titulaire

Christian GORINI, Professeur à l'Institut des Sciences de la Terre (ISTEP) - UMR 7193 -UMPC-CNRS, nous a remis une lettre de motivation ainsi qu'un CV qui ont été soumis aux membres titulaires présents. Sa candidature a été acceptée à l'unanimité des présents.

Candidature Pavle ANDJUS en tant que membre correspondant

Pavle ANDJUS, Professeur Titulaire en Physiologie et Biophysique à l'Université de Belgrade (Serbie) nous a remis une lettre de motivation ainsi qu'un CV qui ont été soumis aux membres titulaires présents. Sa candidature a été acceptée à l'unanimité des présents.

L'AEIS se réjouit d'accueillir ces deux nouveaux membres .

II. Conférence

A. Présentation du conférencier Daniel ESTÈVE,

Daniel ESTEVE, né le 2 février 1954, est Directeur de Recherche au CEA à la tête du du groupe de Quantronique (*Quantronics*)du SPEC au CEA Saclay. Son groupe de recherche est dédié à l'étude des circuits électriques quantiques et plus largement à la physique mésoscopique. Il est également membre de l'Académie des Sciences.

Ses travaux principaux traitent de l'effet tunnel quantique d'une jonction de Josephson, de dispositifs à électron unique dans lesquels les électrons sont transférés un par un de manière contrôlée , du blocus dynamique de Coulomb de l'effet tunnel qui a conduit à l'électronique individuelle et à l'électronique de paire individuelle de Cooper, aux échanges énergétiques entre les électrons des circuits mésoscopiques qui déterminent leur cohérence quantique, la supraconductivité de proximité dans les nanostructures , le processus d'information quantique avec circuits de bits quantiques supraconducteurs, l'ESR à la limite de sensibilité quantique; l'optique quantique avec des photons à microondes . La Quantronique a démontré d'abord qu'un circuit électrique quantique était capable de reproduire les expériences fondamentales de la physique quantique réalisées longtemps avant avec les atomes. La Quantronique a obtenu une démonstration de principe de l'accélération quantique d'un algorithme quantique avec un processeur quantique élémentaire supraconducteur. La Quantronique développe actuellement des structures hybrides basées sur des circuits supraconducteurs quantiques combinés avec des spins.

Il est membre de l'Académie des Sciences, du Comité éditorial PRX et du Conseil scientifique du LNE 5laboratoire National de Métrologie et d'Essai). Il a été élu vice- Président de l'ERC de 2007 à 2012. Il a reçu lui-même et en collaboration avec d'autres diverses récompenses telles le prix *Agilent Europhysics* pour le développement du premier dispositif électrique fonctionnel à bit quantique et le Grand Prix Ricard de la SFP.

B. Résumé de la conférence

Des Circuits électroniques quantiques

par Daniel ESTÈVE

Tout système physique étant capable en théorie d'atteindre le régime quantique , la recherche des propriétés quantiques des systèmes non-microscopiques s'est considérablement développée pour les variables mécaniques ou les nano-objets et pour les variables électriques des circuits supraconducteurs non dissipatifs.

La découverte au milieu des années 90 selon laquelle la mécanique quantique fournit des moyens de réalisation de tâches de calcul dépassant celles des ordinateurs classiques a provoqué une recherche intense dans le domaine des unités de base, nommément les circuits de bits quantiques nécessaires à la réalisation d'un ordinateur quantique. Je décrirai les bits quantiques les plus avancés et les processeurs quantiques élémentaires réalisés avec. J'expliquerai le problème de flexibilité (scalabilité) pour réaliser un ordinateur quantique intéressant et les solutions envisageables. J'introduirai une route hybride basée sur les spins microscopiques couplés aux circuits électriques quantiques qui sont développés actuellement dans notre équipe.

.

Un compte-rendu rédigé par un membre de l'AEIS sera prochainement disponible sur le site de l'AEIS http://www.science-inter.com.

REMERCIEMENTS

Nous tenons à remercier vivement M. Jean-Louis DUPLOYE et M. Yann TRAN de l'Institut Curie pour la qualité de leur accueil.

Annonces

Nous vous rappelons l'**annonce de notre prochain colloque** . Pour vous inscrire il suffira de vous rendre sur le site **https://aeis-2020.sciencesconf.org/ .**

AEIS-2020
LES SIGNATURES DES ÉTATS MÉSOSCOPIQUES DE LA MATIÈRE

Jeudi 12 et vendredi 13 mars 2020

Amphithéâtre Constant Burg - Institut Curie
12 rue Lhomond - 75005 Paris
https://aeis-2020.sciencesconf.org/

L'Académie Européenne Interdisciplinaire des Sciences (AEIS Paris) prépare son prochain colloque interdisciplinaire et européen aeis-2020 sur le thème « LES SIGNATURES DES ÉTATS MÉSOSCOPIQUES DE LA MATIÈRE ».
Ce colloque aura pour ambition de faire le point sur quelques avancées significatives sur des propriétés de la matière à une échelle intermédiaire entre l'échelle macroscopique qui caractérise les corps dans leur ensemble à notre échelle métrique et l'échelle microscopique qui caractérise les atomes et les molécules avec leurs nombreuses applications. La physique mésoscopique s'intéresse aux propriétés de la matière condensée qui apparaissent à une échelle intermédiaire entre la physique classique et la physique statistique d'une part et la physique quantique d'autre part. La chimie mésoscopique concerne notamment les nanomatériaux et les méso-cristaux. La chimie mésoscopique recouvre à la fois la synthèse et l'étude des modes de construction d'objets chimiques ayant des tailles dans cette échelle intermédiaire (2 nm-1µm), l'assemblage bidimensionnel ou tridimensionnel d'objets bien définis situés dans cette gamme de taille et l'étude des propriétés physiques des matériaux résultants. En Biologie l'exploration de cette nouvelle dimension entre le micron et le nanomètre conduit à repenser radicalement la compréhension que l'on avait de nombreux phénomènes biologiques. … Il s'agit là d'une véritable « *Biologie mésoscopique* » où sont révélées de nouvelles propriétés des systèmes vivants, propres à cette échelle. » (Antoine Triller) ……
Disciplines : Chimie, Physique, Sciences du vivant
Il se déroulera sur deux jours et aura lieu à l'Institut Curie les jeudi 12 et vendredi 13 mars 2020. Il comportera quatre sessions (http://www.science-inter.com/)

Informations pratiques

1. **En cas de difficultés d'inscription adresser un mail à iherpelitwin@gmail.com**

Plan Amphi. BURG http://www.francepathol.org/dyn_img/congres_file_243_3.pdf

ACADÉMIE EUROPÉENNE INTERDISCIPLINAIRE DES SCIENCES
INTERDISCIPLINARY EUROPEAN ACADEMY OF SCIENCES

Colloque AEIS-2020
LES SIGNATURES DES ÉTATS MÉSOSCOPIQUES DE LA MATIÈRE

Jeudi 12 et vendredi 13 mars 2020
Amphithéâtre Constant Burg - Institut Curie
12 rue Lhomond - 75005 Paris

PROGRAMME PRÉVISIONNEL

Jeudi 12 mars 2020 matin : allocution + session 1

Plage horaire	*activité*
9h-9h25	Allocution représentants AEIS remerciements Institut Curie
9h25-10h	**Gwendal FÈVE** Sorbonne Université, Laboratoire de Physique Pierre AIGRAIN de l'ENS Ulm ***Électronique quantique dans les nanoconducteurs***
10h-10h10	Échanges avec assistance
10h10-10h45	**Christophe MORA** Université Paris Diderot (Paris 7) Laboratoire de Physique Pierre AIGRAIN de l' ENS Ulm ***Topologie et physique quantique mésoscopique***
10h45-10h55	Échanges avec assistance
10h55-11h10	PAUSE
11h10-11h45	**Daniel ESTÈVE** Membre de l'Académie des Sciences Service de Physique de l'État Condensé CEA-Saclay Groupe Quantronique Ordinateur quantique ***circuits mésoscopiques quantiques***
11h45-11h55	Échanges avec l'assistance
11h55-13h45	PAUSE déjeuner

Jeudi 12 mars après-midi : session 2

Plage horaire	*activité*
13h45-14h20	**Clément SANCHEZ** Membre de l'Académie des Sciences Chaire de « Chimie des Matériaux Hybrides », Collège de France Chimie de la Matière Condensée de Paris, UMR 7574-UPMC/CNRS/Collège de France **À venir**
14h20-14h30	Échanges avec l'assistance
14h30-15h05	**Sandrine SAGAN** Directrice Laboratoire des BioMolécules LBM UMR 7203 ENS-Ulm - Laboratoire des BioMolécules ***Progrès récents dans le transport de molécules au travers des membranes cellulaires, ou comment des molécules polaires de haut poids moléculaire peuvent traverser une barrière imperméable sans systèmes de transport spécialisés***
15h05-15h15	Échanges avec l'assistance
15h15-15h30	PAUSE
15h30-16h05	**Rodolphe VUILLEUMIER** **Sorbonne Université** ENS-Ulm - Département de chimie ***Simulations de dynamique moléculaire: un microscope numérique pour sonder la matière à l'échelle atomique***
16h05-16h15	Échanges avec l'assistance
16h15-16h50	**Jean-François DUFRÊCHE** Laboratoire Modélisation Mésoscopique et Chimie Théorique (LMCT) Institut de Chimie Séparative de Marcoule ICSM UMR 5257 /CEA / CNRS / Université de Montpellier / ENSCM ***Modélisations multiéchelles pour la chimie à l'échelle mésoscopique : l'exemple de la chimie séparative***
16h50-17h	Échanges avec l'assistance

Vendredi 13 mars 2020 matin: Session 3

Plage Horaire	activité
9h30 -10h05	**Antoine TRILLER** Membre de l'Académie des Sciences Institut de Biologie de l'École Normale Supérieure ENS. CNRS UMR8197. Inserm U1024 ***Biologie quantitative de la communication entre neurones : instabilité moléculaire et mémoire, du normal au pathologique***
10h05-10h15	Échanges avec l'assistance
10h15-10h50	**Terence STRICK** Professeur et chef d'équipe Nanomanipulation de biomolécules Institut Jacques Monod Université Paris Diderot Institut de Biologie de l'ENS (IBENS) ***Il y a plus de marge de manœuvre en bas de l'échelle : vers un détecteur universel des interactions moléculaires***
10h50-11h	Échanges avec l'assistance
11h-11h15	**PAUSE**
11h15-11h50	**Vincent HAKIM** Équipe "Biophysique et neuroscience théoriques" Laboratoire de Physique de l'École Normale Supérieure (LPENS) & CNRS ***Énigmes concernant la mémoire à long-terme et l'apprentissage***
11h50-12h	Échanges avec l'assistance
12h-13h45	**PAUSE déjeuner**

Vendredi 13 mars 2020 après-midi: Session 4

Plage Horaire	activité
13h45-14h20	**Mathieu COPPEY** Chef d'équipe Imagerie et contrôle de l'organisation cellulaire (LOCCO) UMR168 – Laboratoire Physico-Chimie Institut CURIE ***Organisation spatiale et temporelle à l'échelle mésoscopique d'une protéine de signalisation cellulaire***
14h20-14h30	Échanges avec l'assistance
14h30-14h45	**Pause**
14h45-15h20	**Olivier HAMANT** Laboratoire de Reproduction et développement des plantes École Normale Supérieure (ENS) de Lyon ***Des systèmes et matériaux (ré)actifs chez les plantes***
15h20-15h30	Échanges avec l'assistance
15h30-16h00	**Remerciements et clôture**

Documents

Pour préparer la conférence d'Olivier HAMANT :

p.12 : le résumé en français de sa présentation

p.13 : Un article intitulé "*Are microtubules tension sensors?*" d'Olivier HAMANT, Daisuke INOUE, David BOUCHEZ, Jacques DUMAIS et Eric MJOLSNESS, publié dans Nat Commun. 2019; 10: 2360. accessible sur le site : https://www.ncbi.nlm.nih.gov/pmc/articles/PMC6541610/

p. 25 : Un article intitulé " *A tension-adhesion feedback loop in plant epidermis*" par Stéphane Verger, Yuchen Long, Arezki Boudaoud, et Olivier Hamant publié le 23 avril 2018 . doi: 10.7554/eLife.34460 sur le site https://www.ncbi.nlm.nih.gov/pmc/articles/PMC596392

.

Des systèmes et matériaux (ré)actifs chez les plantes

par Olivier HAMANT
Directeur de Recherche à l'INRA
Laboratoire de reproduction et développement des Plantes /ENS Lyon

Les systèmes vivants sont aussi des objets physiques. Contrairement aux animaux en développement, constitués de cellules mécaniquement souples et contractiles, les tissus des plantes en croissance sont très rigides et fortement pressurisés. L'immobilité résultante des plantes pourrait faire croire à une absence de réaction des constituants cellulaires végétaux aux contraintes mécaniques. Des résultats obtenus ces dernières années démontrent au contraire le caractère très réactif des plantes, et des matériaux les constituant, à toutes les échelles. Dans ce séminaire, l'exemple de la dynamique de la synthèse de cellulose nous permettra de mettre en évidence le rôle des forces dans la morphogenèse des plantes.

nature COMMUNICATIONS

PERSPECTIVE

https://doi.org/10.1038/s41467-019-10207-y OPEN

Are microtubules tension sensors?

Olivier Hamant[1], Daisuke Inoue[2], David Bouchez[3], Jacques Dumais[4] & Eric Mjolsness[5]

Mechanical signals play many roles in cell and developmental biology. Several mechanotransduction pathways have been uncovered, but the mechanisms identified so far only address the perception of stress intensity. Mechanical stresses are tensorial in nature, and thus provide dual mechanical information: stress magnitude and direction. Here we propose a parsimonious mechanism for the perception of the principal stress direction. In vitro experiments show that microtubules are stabilized under tension. Based on these results, we explore the possibility that such microtubule stabilization operates in vivo, most notably in plant cells where turgor-driven tensile stresses exceed greatly those observed in animal cells.

Mechanical forces are increasingly viewed as instructive signals for many cell biology processes, such as cell polarity[1], division[2], and fate[3]. Mechanical forces also play important roles in developmental biology. For instance, tissue folding during gastrulation in Drosophila[4] or during organogenesis in plants[5] involves a response of the cytoskeleton to mechanical forces. Similarly, the mechanical conflicts associated with differential growth in organs constrain their final shape, both in animals[6,7] and plants[8]. Several mechanotransduction pathways have been identified[9], yet there is no clear mechanism for sensing stress direction so far. Typically, membrane tension is thought to open mechanosensitive channels, through membrane thinning[10]. However, the plasma membrane is fluid, and thus can only be under isotropic tension, like a soap film. The transmission of stress direction through the membrane requires a coupling with an elastic solid, such as the cell wall, the extracellular matrix, or the cortical cytoskeleton. Because cytoskeletal proteins are structurally and dynamically directional, they may be inherently more sensitive to the directionality of mechanical cues. Interestingly, the cytoskeleton has been proposed to respond directly to mechanical stimuli, making this structure not only a good substrate for the transmission of mechanical information but also a potential contributor to the transduction of stimuli. For instance, in single cells, tension modifies formin conformation, from an inhibitory to a permissive one, thereby promoting actin polymerization[11], whereas compression can promote actin branching, thereby affecting the contractile behavior of the cell cortex[12].

More generally, to sense direction, one needs an anisotropic probe. Microtubules may be particularly well-suited for this function not only because their shape makes them typically anisotropic, but also because these molecules are remarkably stiff. In fact, the 25 nm-wide microtubules are three orders of magnitude stiffer than actin[13], endowing them with a high persistence length and the ability to maintain their shape and anisotropy. Furthermore, and maybe more importantly, the bending stiffness of microtubules allows them to maintain a given

[1] Laboratoire de Reproduction et Développement des Plantes, Université de Lyon, UCB Lyon 1, ENS de Lyon, INRA, CNRS, 46 Allée d'Italie, 69364 Lyon Cedex 07, France. [2] Cell and Plant Physiology Laboratory, CytoMorpho Lab, CEA, Biosciences and Biotechnology Institute of Grenoble, 38054 Grenoble, France. [3] Institut Jean-Pierre Bourgin, INRA, AgroParisTech, CNRS, Université Paris-Saclay, 78000 Versailles, France. [4] Facultad de Ingeniería y Ciencias, Universidad Adolfo Ibáñez, Viña del Mar, Region V, Chile. [5] Departments of Computer Science and Mathematics, University of California, Irvine, CA 92697-3435, USA. Correspondence and requests for materials should be addressed to O.H. (email: olivier.hamant@ens-lyon.fr)

direction over the whole cell or at least a large part of it. Thus, the mechanical properties of microtubules, together with their extended shape, make them well-suited to perceive cell-scale mechanical signals.

Here, in the spirit of a perspective, we explore the possibility that individual microtubules are able to sense their own longitudinal tensile status, and to align spontaneously with the direction of maximal tensile stress (mathematically, the principal axis of the stress tensor, in living cells and tissues; key terms are defined in Box 1).

Plants are ideal systems to study this question for two main reasons. First, turgor pressure in plant cells routinely exceeds 0.5 MPa, which builds up high tensile stresses at the cell cortex, where a dense population of microtubules (so-called cortical microtubules, CMTs) self-organize in a confined 2D space. Second, there is overwhelming evidence that plant cortical microtubules respond quickly to changes in the stress in plant cells[5,14,15]. Therefore, by virtue of their extended nature, their high persistence length, their position at the cell cortex, and their rapid response to changes in wall stresses, microtubules are the best candidate as the cellular structure able to sense the direction of stress.

Note that because of the presence of stiff cell walls, the only origin of mechanical stress in plant cells is turgor pressure. Spindle microtubules are known to generate a pushing or pulling force when they grow or shrink, respectively. However, such forces are small: the addition of 13 dimers (i.e., a full 8 nm tall ring of tubulin dimers) is thought to generate a force of ~50 pN[16]. Given that the stiffness of cell walls is in the MPa range, such forces are negligible. In fact, plant cells do not change their shape for several hours after microtubules have been depolymerized[17,18].

How could microtubules align with the direction of maximal tension? Does this response require a specific mechanotransduction pathway? Plant microtubules are comparable to microtubules found in animal systems[19,20], although they exhibit increased dynamics: using purified plant tubulin assembled in vitro, catastrophe was found to be more frequent than in animals and the shrinking rate was almost 10 times higher in plants than in animals (195 µm/min for plant microtubules vs. 21 µm/min for animal microtubules)[21]. γ-TuRCs are located both at the nuclear envelope and the plasma membrane, yet, the plasma membrane is generally thought to be a dominant site for microtubule nucleation, at least during interphase[22,23]. The alignment of CMTs with tension likely involves self-organization processes (Fig. 1a). Beyond nucleation, CMTs have indeed been shown to form organized arrays spontaneously, through the combination of their (de)polymerization, bundling, and severing[24,25]. Microtubules are dynamic at both plus and minus ends, and the associated bias in dynamic instability results in treadmilling events[26]. Short treadmilling microtubules (0.5–2 µm) represent ca. 90% of the treadmilling microtubules and have a major contribution to the final CMT organization[27]. Although the microtubule lattice is more dynamic than initially anticipated[28], it is now well established that the microtubule ends play a major role in microtubule stability. The SPIRAL2 protein for instance was recently shown to bind and stabilize microtubule minus ends, indirectly impacting the severing rate[23,29]. More directly, tumor overexpressed gene (TOG)-domain containing proteins such as XMAP215 incorporate free tubulin at the microtubule plus ends and thus catalyze microtubule polymerization.

Although the exact contribution of each process to CMT alignment with tension remains to be investigated, katanin-dependent MT severing has been shown to promote CMT alignment with tensile stress[30]. This raises the question of the number and identity of players needed for microtubules to sense tension. In this perspective, we speculate about the most parsimonious hypothesis: could individual microtubules align with rapid changes in maximal tension direction on their own without the help of other factors?

Contribution of cell geometry to microtubule organization

Since tension is borne by the cell walls, the localization of CMTs puts them in the ideal location to sense such cortical cues. Interestingly, the cortical localization of CMTs was recently proposed to emerge from their intrinsic stiffness. When growing geometrically stiff microtubules in a closed 3D space and allowing them to self-organize in arrays in silico, they tend to populate the cortex of the cell: when microtubules reach the cell membrane, they may grow in the plane of the membrane without returning to the cell volume; the cell surface thus acts as a microtubule sink in a positive feedback loop[31] (Fig. 1b). Although this obviously does not exclude anchoring molecules (Box 2), microtubule localization already exhibits a bias that makes them more prone to sense cortical signals on their own. Interestingly, when animal cells differentiate, they tend to loose their centrosome, and this is accompanied by an increase in the cortical localization of microtubules[32] (Fig. 1c), also consistent with the model's prediction. The increased density of nucleating proteins, such as GCP proteins and pre-existing microtubules[22,33], would further confine microtubules to the cell cortex.

In the above-mentioned 3D model of MT self-organization, and confirming previous work, CMTs were shown to be sensitive to cell geometry and to align with the long axis of the cell[31] (Fig. 2a). At the individual microtubule level, high persistence length would make them avoid the curvy parts of the cell. As they self-organize into complex arrays, such bias would be sufficient to generate microtubule networks aligning along the straightest parts of the cell, i.e., along the longest wall of a plant cell. Several in vitro assays in cell-sized microchambers also reproduced microtubule orientation along the longitudinal axis of such confined space (Fig. 2b[34,35]). Detailed analysis of microtubule behavior in *clasp* mutant further supports this view: CLIP170-

Box 1 | Definitions

- Stress (σ): a force per unit area upon which the force is acting (measured in Pa). Stress is also the mathematical product of stiffness and strain ($\sigma = E\varepsilon$).
- Strain (ε): a normalized and unitless measure of deformation (in 1D for an object of length l, $\varepsilon = (l - l_0)/l_0$).
- Stretch (η): a unitless measure of deformation (in 1D for an object of length l, $\eta = l/l_0$).
- Stiffness (E): a measure of the rigidity of the material. E corresponds to the elastic modulus of the material (in Pa). $E = \sigma/\varepsilon$.
- Persistence length: a measure of the stiffness of a linear polymer, as the length over which correlations in the direction of the tangent are lost.

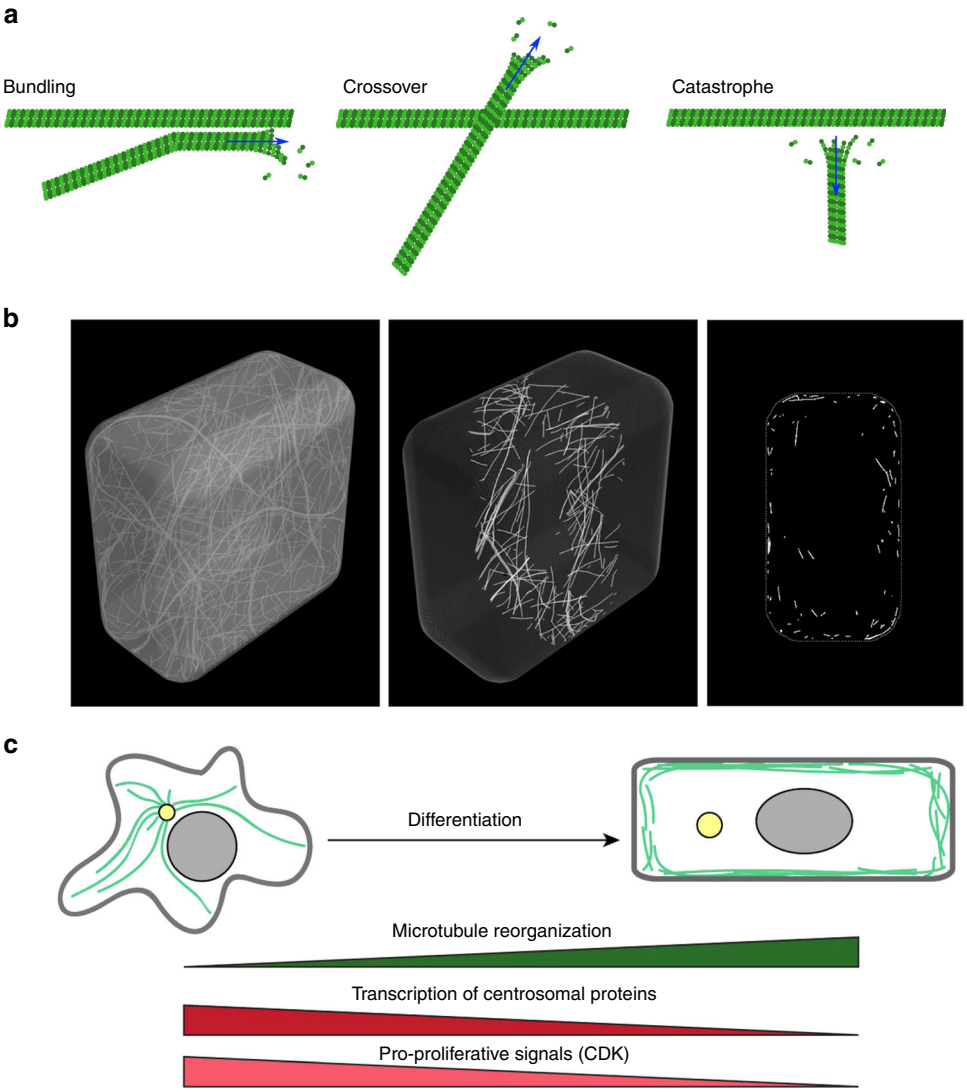

Fig. 1 Microtubule self-organization properties lead to their cortical localization by default. **a** Dynamic instability and self-organizing properties of microtubules. Bundling occurs for collision angles inferior to 40°; for larger angles, induced catastrophes or crossover occur. **b** Microtubules are cortical by default in silico (adapted from ref. [31]). **c** Upon centrosome disorganization, microtubules can become cortical in differentiated animal cells (adapted from ref. [32])

associated protein (CLASP) has indeed been proposed to help microtubules continue to polymerize as they bend around sharp cell edges; in the *clasp* mutant, increased rate of catastrophe is measured at cell edges thereby constraining the final CMT alignment[36]. Cell geometry is thus a contributor to CMT organization in plant cells.

However, computational modeling predicts that this bias may be weak. To test whether the microtubule alignment according to cell shape is robust, the growth direction of microtubules was biased in silico: growth occurs from the microtubule plus end with a small directional noise; when this noise was biased by a cue in a direction other than the longitudinal axis, with a weight of ~ 1% only, the final CMT orientation in virtual cells followed the direction of that bias[31] (Fig. 2a). This study does not exclude a contribution of cell geometry in CMT orientation; in fact, it suggests that CMT orientation is determined by cell geometry by default (i.e., in the absence of another, prevalent cue). However, this model suggests that cell geometry is not a strong determinant of CMT orientation. This would be consistent with the observation that adjacent cells can exhibit consistent CMT co-alignment, despite having different shapes[5]; conversely, cell geometry would add noise to neighboring cells with different shapes if supracellular stress were not strongly anisotropic.

Interestingly, in the absence of strong supracellular cues, cell geometry would in fact be sufficient to bias the pattern of mechanical stress in the wall. Typically, for a single pressurized elongated cell, maximal tension is transverse to the long axis of the cell[37] (Fig. 2c). Using finite element models, the subcellular pattern of stress in the outer walls of adjacent cells in the epidermis was calculated[38,39]: tension in the (outer) wall should be twice higher along the circumference than along the long axis of the cell whether the cell is isolated or in a tissue. Therefore, when including the mechanical implications of cell geometry, and assuming that CMTs would align with maximal tension, such a cue may in principle be enough to override the purely steric impact of local curvature and cell shape on the final CMT array alignment.

Microtubule stabilization by tension in in vitro assays

Is there any evidence that microtubules can align with tension on their own? Several in vitro studies have addressed this issue. In

Box 2 | Putative anchoring mechanisms for CMTs

Whereas the extracellular matrix–plasma membrane–actin continuum is rather well described and understood in animal cells, the exact nature of the cell wall–plasma membrane–CMT continuum is largely unknown in plants. Several proteins connecting the plasma membrane and the cytoskeleton have been identified[92–94] and the lateral movement of several plasma membrane proteins is constrained by their interaction with the cell wall[95]. Electron microscopy and total internal reflection fluorescence microscopy images clearly show that microtubules are anchored to the plasma membrane. Conversely, when a microtubule end detaches from the membrane, it becomes quite agitated owing to active cytoplasmic streaming underneath (see e.g.[96]). Physical links between the plasma membrane and the cell wall are easily visualized upon partial plasmolysis, forming the so-called "Hechtian strands". Such anchoring points are usually associated with plasmodesmata. As their number is relatively low, and despite the high bending stiffness of microtubules, plasmodesmata anchoring points would not be sufficient to explain the attachment of all CMTs to the plasma membrane. A second, non-exclusive, mechanism involves proteins that bind both microtubules and phospholipids. For instance, phosphatidic acid can recruit MAP65, which binds and bundles microtubules[97]; PIP2 biosensors have also been reported to accumulate in mechanically stressed regions where CMTs are stably co-aligned[98]. Such interactions may provide a relatively direct membrane anchoring mechanism: the fluidity of the membrane would allow a degree of freedom in CMT reorientation, and the CMT self-organization together with the indirect connection of the CMT network to fixed points (plasmodesmata), could maintain a stable cell wall–plasma membrane–CMT continuum. Note here that, at the plasma membrane, several receptor-like kinases exhibit an Arg-Gly-Asp (RGD)-binding motif, which may bind wall components, in a way analogous to integrins in animal cells binding to fibronectin RGD motifs[99]. Consistent with this idea, the plasma membrane tends to detach from the cell wall upon treatment with free RGD peptides[100]. Last, as CMTs are indirectly bound to the cellulose synthase machinery through CSI[101] and CMU[102] proteins, CMTs may also be anchored to the membrane in part via the cellulose synthesis machinery

gliding assays, where stable microtubules are propelled by surface-anchored motor proteins (kinesin and dynein), populations of microtubules move toward random directions on a planar surface, which mimics the displacement of CMTs. Recently, thanks to a coupling between stretchable polydimethylsiloxane (PDMS) substrate and the conventional gliding assay system, when microtubules gliding on a PDMS were subjected to tension by elongation of the substrate, the randomly moving microtubules aligned themselves along the tension lines. As the application of tensile stress was transient, orientation of microtubules became random soon after the release of tension. Conversely, microtubules that were put under compression in the same set-up re-aligned to be orthogonal to maximal compression direction (Fig. 3a, b). However, when stationary microtubules were subjected to tensile or compression stress, they underwent fragmentation and buckling, respectively[40] (Fig. 3c). These results suggest that microtubules are able to reorganize when the stress pattern undergoes rapid changes and self-organize in aligned arrays in the direction of maximal stretch.

In polymerization assays of microtubules where microtubules growth is catalyzed by tiny stabilized microtubules (so-called seeds), the growing end of microtubules stretched by optical tweezers were found to prominently grow under tension[41,42] (Fig. 3e). More specifically, beads coated with a kinetochore protein (Dam1), which stably binds microtubule ends, were attached at microtubule ends, trapped and then pulled using an optical tweezer. Microtubule shrinking rate was reduced to one third of its initial value (from 158 nm/s to 56 nm/s) when the applied tensile force was increased from 0.5 to 2 pN, showing that tension can slow down microtubule depolymerization. Note that when switching between different force regimes, with abrupt changes in force magnitude, microtubule shrinking rate was also immediately affected. This suggests that the effect of tension on microtubule is direct and that microtubules are able to perceive changes in force magnitude. Using a similar strategy, albeit using XMAP215-coated beads, the mean polymerization rate was twice higher when the pulling force was ~1 pN when compared with forces smaller than 0.5 pN. This demonstrates that tension promotes the polymerization activity of XMAP215 on microtubules. Interestingly, like XMPA215, both microtubule organizer1 (MOR1) and CLASP in plants contain plus end stabilizing TOG domains, and thus are in good positions to affect microtubule polymerization in a force-dependent way.

Altogether, these in vitro studies suggest that the tension experienced by a microtubule can have a determining effect on the microtubule spontaneous behavior. How stress is sensed is a question that must be addressed both by computational scientists and structural biologists. For instance, an in silico study disclosed that microtubule orientation is biased by applied mechanical stimuli in order to minimize the accumulated bending energy in the microtubule shaft under compression of the substrate[43] (Fig. 3d). Here we formulate a simple energy-based mathematical model of tension sensing in a single microtubule end, based on a one-dimensional two-state mechanical model of tubulin protofilament alignment as illustrated in Fig. 4. A macroscopic mechanical analogy for this model could be made to the two states of a hemispherical deflated ball: side A outside and side B inside (state $s = 0$), or vice versa (state $s = 1$). Parameter μ_s represents the difference in mechanical energies between the two states, and controls which state (if either) has the lower energy and the higher probability. Note that energy differences at this molecular scale would be comparable to thermal energy fluctuations. Using such a model one can evaluate the free energy associated with each value of an externally imposed tension τ. The result is a double-well potential, with one local minimum energy near $\tau = 0$ corresponding to the splayed state of microtubule protofilament sheets and another local minimum for larger τ corresponding to the aligned state of microtubule protofilaments, whether the input is biochemical (GTP hydrolysis) or mechanical (imposed tension). In this way, external tension could indeed stabilize the aligned state of the MT end cap. At the molecular level, one may check whether the aligned state promotes the recruitment or activity of XMAP215, which would then catalyze tubulin subunit incorporation.

Recent progress in cryoEM may help us relate microtubule dynamic instability and mechanical stress within the lattice[44]. For instance, high-resolution images reveal that GTP hydrolysis changes the conformation of α-tubulin, leading to tubulin dimer compaction along the axis of protofilaments, and thus generating tension in the lattice[45,46]. Although it remains to be explained how external tension can interfere with this structural response, microtubule stability may very well depend on their tensile status. In other words, we are now closer to causally linking the intrinsic structure of the microtubule to its ability to withstand tension, while being destabilized by compression. This mechanical asymmetry, together with their elongated, anisotropic, shape, could be sufficient to make them tension sensors on their own.

Cell wall contribution to the CMT response to stress

Based on the in vitro experiments discussed above, microtubules are stabilized by tension. In the simplest in vivo scenario, changes in

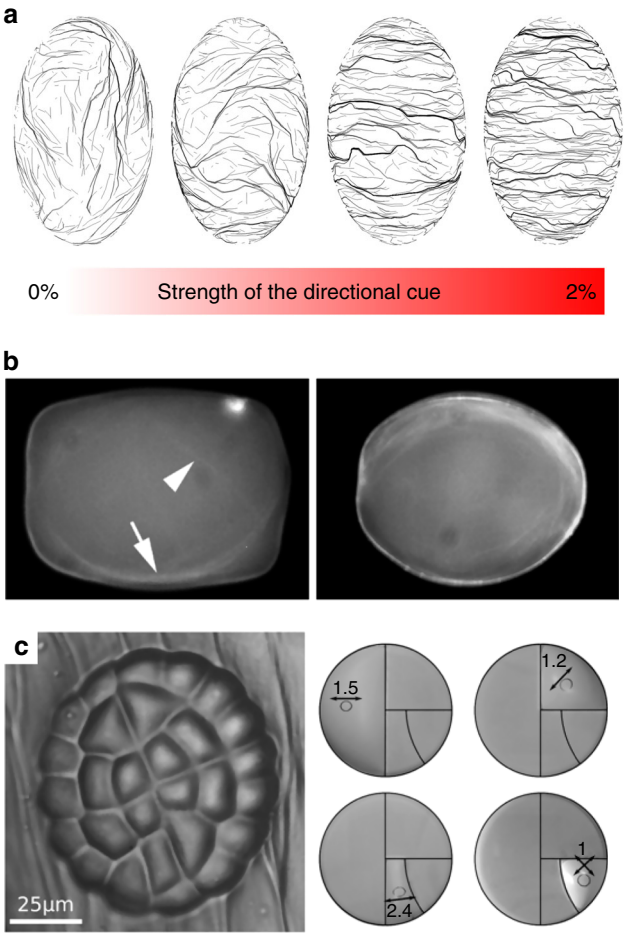

Fig. 2 Microtubules are sensitive to cell geometry. **a** In silico, microtubule-bending stiffness weakly influences their final alignment towards the longitudinal axis of the cell; cell geometry also prescribes maximal tension along the transverse direction of the cell, which may in turn counteract the effect of confinement on the final microtubule configuration (adapted from ref. [31]). **b** In vitro, microtubules can align with the longitudinal axis of confined spaces. In the present study, most (71%), rhodamine-labeled microtubules aligned along the longitudinal axis of confined space in vitro after 1 h of incubation at room temperature (adapted from ref. [34]). **c**. Left division pattern in the glandular trichome of *Dionaea muscipula;* right: predicted maximal tension directions in the membranes (deformed circles) matching division planes (adapted from ref. [89])

external tension from the cell wall would be transferred to microtubules. This is by far the strongest assumption of this article, for at least two reasons. First, the wall–membrane–microtubule continuum is ill-described (Box 2). Second, the tension-induced fragmentation of immobilized microtubules on stretched PDMS[40] appears to be incompatible with the idea that wall tension stabilizes cortical microtubules in plant cells. At this stage, we can assume that the wall–membrane–microtubule continuum allows a certain degree of freedom for CMTs to keep some motility. Consistent with this assumption, electron microscopy data show that cortical microtubules in leaf epidermal cells can detach from the plasma membrane and, in such situation, they align with the longitudinal axis of the cell, which fits both constraints imposed by cell geometry (see Fig. 2) and the main shear stress imposed by cytoplasmic streaming. Interestingly, such behavior happens when cells have ceased to elongate, or when cells are treated with 1-butanol, which likely affects the microtubule anchoring to the plasma membrane[47].

Before testing the hypothesis that microtubules can respond to changes in tensile stress direction in a real plant cell, experiments in wall-less protoplasts may provide some interesting indications. In particular, when protoplasts are stretched by centrifugation, CMTs align with the direction of maximal tensile stress[48]. However, such experiments may not be conclusive enough for our purpose, as they do not clearly distinguish the impact of cell geometry, cell strain, or stress. For instance, one could imagine that CMTs acquire their default organization along the new longitudinal axis of the protoplast, or that microtubules become parallel to maximal strain, rather than maximal tensile stress. Interestingly, in animal cells, non-spindle microtubules can also respond to similar deformations: they notably populate the leading edge of experimentally stretched fibroblasts, aligning with the directional of maximal stretch[49], consistent with the CMT orientation in plant protoplasts stretched by centrifugation. However, it again remains difficult to distinguish the microtubule response to stress from other cues, such as strain or geometry. These examples highlight the need to clearly differentiate the putative contributions of stress and strain to microtubule dynamic behavior. Plant cells may offer a way to do this.

In a plant cell, the maximal direction of (plastic) strain (i.e. growth) is often perpendicular to the predicted direction of maximal tensile stress, because of the anisotropic properties of the cell wall. Indeed, cortical microtubules generally guide the trajectory of cellulose synthase complexes at the plasma membrane[17,50]. This implies that when microtubules align with tension, they also indirectly resist tension, through the synthesis of cellulose microfibrils in the maximal direction of tensile stress in the wall[5,14]. In the vast majority of cells, the tensile stress patterns are anisotropic. If CMTs align along maximal tensile stress directions, then the anisotropic reinforcement of the wall through the deposition of cellulose microfibrils would reduce stress in that direction during growth, possibly until stress in the formerly minimal direction becomes higher and CMT orientations are randomized or switch to the next maximal stress direction. Altogether, this means that the relation between microtubules, strain and tensile stress is more complex in plants, as plant cells tend to grow in a direction that is orthogonal to maximal tension. Consequently, in contrast to protoplasts, walled plant cells offer the unique opportunity to discriminate between the microtubule response to strain or stress.

CMTs align with maximal tensile stress in plant tissues

CMTs are usually perpendicular to the maximal growth direction (maximal strain) and they usually align parallel to predicted maximal tensile stress direction in plants. This has been repeatedly observed by different teams[5,15,51,52], in different tissues (protoplasts[48], epidermal peels[15], hypocotyls[52,53], shoot meristems[5], cotyledons[38], leaves[51], immature seeds[54], stems[53], sepals[8]), at different scales, from subcellular[38] to multicellular[5], and using different micromechanical tests (stretching[15,52], compression[5,51,55], ablation[5], drugs[30]) (Fig. 5). Note that the only cases where CMT orientation is not consistent with tensile stress pattern are in asymmetrically dividing cells (where an arc-shaped microtubule structure, the preprophase band, marks the next division site) and arguably in young hypocotyls, which exhibit constant rotations of their CMTs[56].

In the following, we focus on cells at the shoot apical meristems where microtubule behavior has been analyzed, mechanical stress pattern has been modeled and several types of micromechanical perturbations have been applied. This tissue also offers a wide range of cell behavior, cells in the central zone growing slowly and isotropically, cells in the peripheral zone growing fast and anisotropically, and cells in the boundary domain growing slowly,

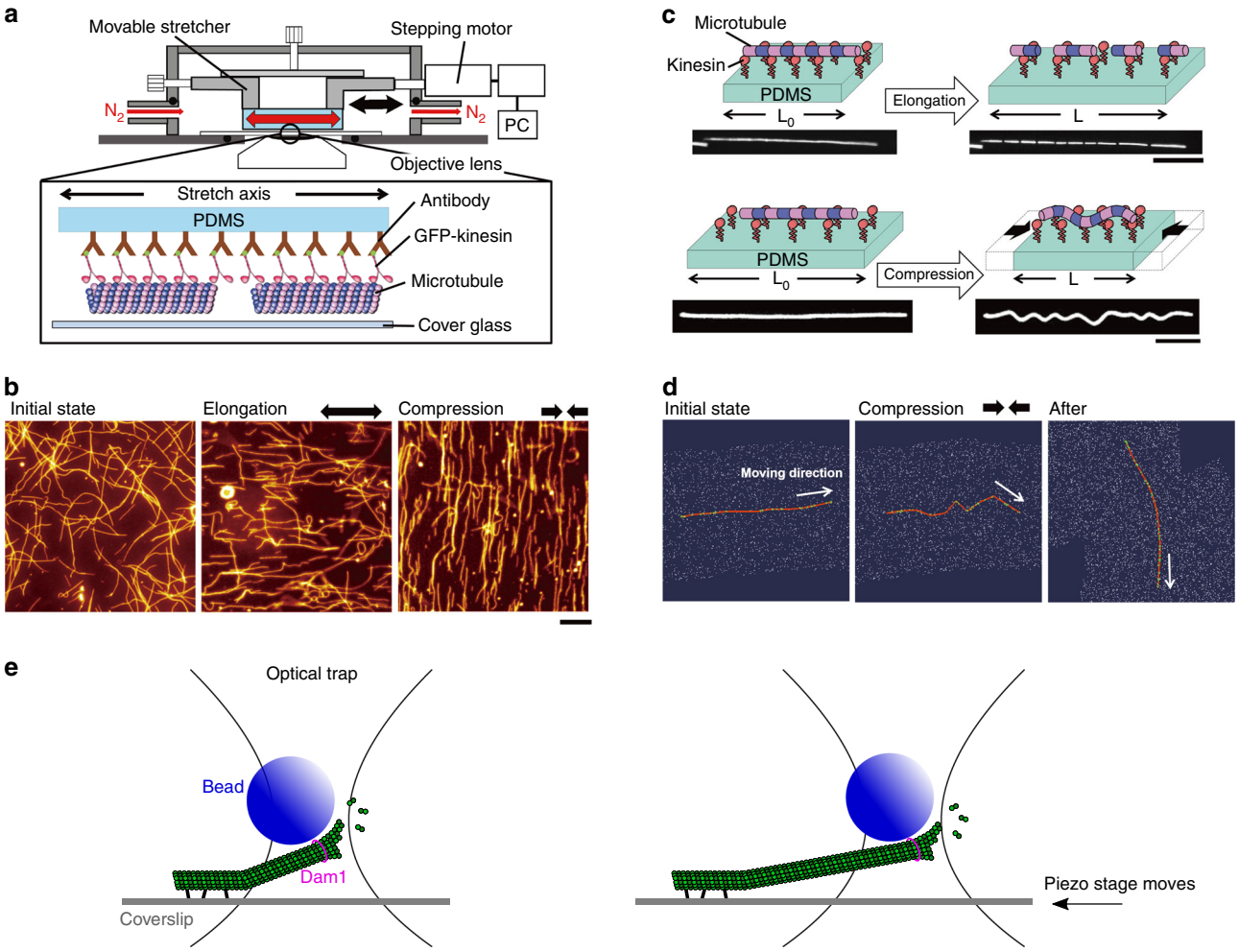

Fig. 3 In vitro microtubules under mechanical stress. **a** Schematic diagram of an in vitro system to apply tension and compression to gliding microtubules on a kinesin-coated elastomer substrate (adapted from ref. [43]). **b** Microtubules driven by surface immobilized kinesins align along maximal tension in vitro and conversely align against compression direction (adapted from ref. [43]). **c** Fragmentation and buckling of microtubules at a stationary state induced by external tension and compression (adapted from ref. [90]). **e** Using optical tweezer, growth of single microtubule is promoted when under tension along the direction of protofilaments (adapted from ref. [41], not to scale). **d** Microtubule aligns toward the direction that minimizes accumulated bending energy in silico (adapted from ref. [43])

being compressed between the organ and the meristem. Meristem cells in Arabidopsis resemble 5 × 5 × 5 µm cubes (±2 µm in the periclinal plane) with an outer cell wall that is about three times thicker than internal walls (300 nm vs. 100 nm). The epidermis is under tension and through indentation experiments, the meristem could be compared with a pressure vessel inflated by a pressure of ~1 MPa[57].

Whereas meristematic cells are roughly isodiametric, CMTs are usually transverse in the peripheral zone and longitudinal in the organ–meristem boundary[5,58] (Fig. 5a), further illustrating that cell geometry is not the sole prescriptor of CMT orientation. Similarly, CMTs are perpendicular to maximal strain direction in the peripheral zone, and parallel to maximal strain direction in the organ–meristem boundary[58]. Maximal strain is thus also unlikely to be a good prescriptor for CMT orientation. In fact, meristematic cell areal growth rate is ~2% per hour on average[30], which, for a 5 µm wide meristematic cell, roughly corresponds to an elongation of 0.4 nm per minute, i.e., five orders of magnitude lower than microtubule growth rate. So far, the only cue that matches CMT orientation in the epidermis of the entire shoot apical meristem is maximal tensile stress: when the stress pattern at the shoot apical meristem is modified either by ablations, compressions or pharmacological treatments, CMTs change their orientation and, within 2 h, follow the new maximal tensile stress direction[5] (Fig. 5b). Interestingly, the CMT response to stress at the shoot apical meristem was also shown to be independent of auxin[59] and calcium[60], thus further supporting the hypothesis that the CMT response to stress, at least in this tissue, may be more direct. If these experiments support the idea that CMTs are able to sense changes in stress direction, they do not necessarily imply that CMTs are also able to sense the stress pattern at steady state. In fact, based on these experiments and the in vitro results, CMTs may primarily sense changes in tensile stress direction.

A shortcoming in all above-mentioned experiments is that the stress pattern is always indirectly inferred: forces are invisible in essence, and cannot be visualized experimentally. Furthermore, most computational and mathematical models of stress are continuous and they focus on the epidermis, which is thought to be the load-bearing layer in most aerial plant organs. Typically, in a pressurized cylinder, maximal tensile stress is twice higher along the circumference, and such stress patterns may apply to stems or petioles. This means that such predictions usually do not take into account the contribution of internal tissues, nor do they consider

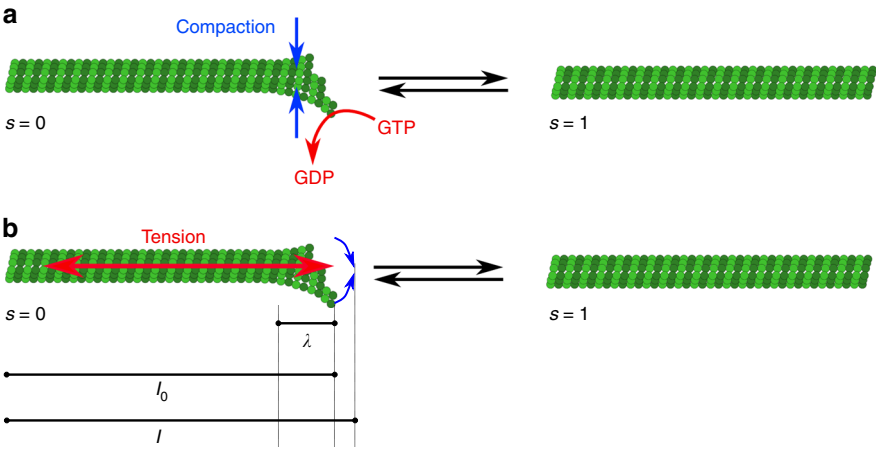

Fig. 4 An energy-based mathematical model of tension sensing in a single microtubule. The model is based on a one-dimensional two-state mechanical model of tubulin protofilament alignment, through GTP hydrolysis **a** or external pulling force **b**, as illustrated. State variables are: the real-valued actual length $l \in \mathbb{R}$ of a stretchable segment of MT (e.g., anchor point to plus end); a binary-valued indicator variable $s \in \{0,1\}$ for the mechanical state of the lengthwise protofilaments at the plus end cap ($s = 0 \Rightarrow$splayed, $s = 1 \Rightarrow$ aligned); and optionally a binary-valued indicator variable $\sigma \in \{0,1\}$ for internal biochemical sensing of the mechanical state s. Principal exogenous parameters are $\lambda \in \mathbb{R}^{\geq 0}$, the length of the splayable subregion; $l_0 \in \mathbb{R}^{\geq \lambda}$, the segment resting length when aligned (so l_0–λ is the resting length when splayed); $\tau =$ externally applied tension; $\mu_s =$ energy bias in favor of (or, if negative, against) alignment $s = 1$; $\mu_\sigma =$ energy bias in favor of $\sigma = 1$; $\alpha =$ energetic reward for agreement of $s = 1$ and $\sigma = 1$. Given this notation, a Hooke's law mechanical spring energy with two states can be written as: $E_{mech} = (k/2)[s(l-l_0)^2+(1-s)(l-(l_0-\lambda))^2]-\tau(l-(l_0-\lambda))$. Additional energy terms specific to discrete end cap state and sensing are: $E_{discrete} = -\mu_s s - \mu_\sigma \sigma - \alpha s\sigma$; then the total energy is $E(l,s,\sigma) = E_{mech}+E_{discrete}$. State probability follows the Boltzmann distribution, $\exp(-\beta E)/Z(\beta,\text{params})$ where Z normalizes the distribution. Even ignoring σ (case α small) one obtains a double-well potential in the free energy $F(\tau) = -(1/\beta)\log Z$ with two minima as a function of tension, one of them near $\tau = 0$. This indicates that nonzero tension can be stabilized by the $s = 1$ mechanical protofilament alignment state which is in turn correlated (for $\alpha \neq 0$) with $\sigma = 1$ tension sensing. The readout state $\sigma = 1$ could in turn be amplified biochemically by, e.g., a phosphorylation/dephosphorylation cycle as in ref. [91], assuming that σ affects such enzymatic activity

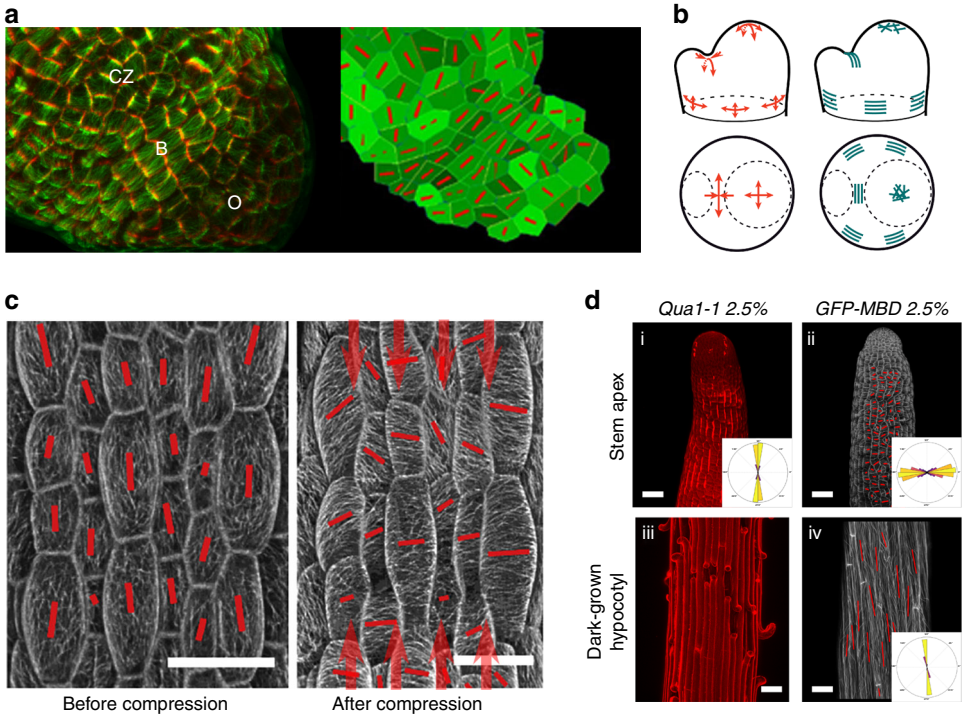

Fig. 5 CMTs align along maximal tensile stress in plants. **a** Left: pattern of cortical microtubules at the shoot apical meristem (CZ: central zone, B: organ–meristem boundary, O: organ). Cell contours (red) and microtubules (green). Right: finite element model where local pattern of stress is predicted, with an emerging co-alignment of tensile stress directions (red bars) at the organ–meristem boundary domain (adapted from ref. [5]). **b** Predicted pattern of mechanical stress at the shoot apical meristem (using a continuous model based on pressure vessel analogy), and matching supracellular microtubule pattern (adapted from ref. [5]). **c** Pattern of cortical microtubules in light-grown hypocotyls before (left) and after (right) controlled compression along the axis of the hypocotyl (adapted from ref. [52]). **d** Correlation between tension pattern derived from adhesion defects (bright propidium staining and cracks) in the *qua1* mutant in stems and basal region of dark-grown hypocotyls (left) and cortical microtubule orientation in a wild-type background (right). Microtubules are revealed by a GFP-Microtubule Binding Domain fusion (GFP-MBD) (adapted from ref. [53])

the small heterogeneities and discontinuities that may alter the local stress pattern. Although these questions remain valid, predicted stress patterns in the epidermis have been indirectly validated by experiments. The load-bearing nature of the epidermis in aerial plant organs was notably revealed by performing cuts, the gaping pattern revealing the presence of tension in that outer layer[61,62]. The primary role of the epidermis in aerial morphogenesis was also further consolidated through molecular genetics experiments in which the whole phenotype of mutant plants can be rescued by expressing the wild-type gene in the epidermis specifically[63,64]. More recently, the tensile stress pattern in several plant organs was revealed, taking advantage of the *quasimodo* mutants, which exhibit cell–cell adhesion defects[53]. By using suboptimal osmotic conditions, such defects could be partially restored, and the direction of the resulting cracks could then be used to derive the anisotropy of tension in hypocotyls, stems, and leaves. Not only this study validated several predicted stress patterns, but it also revealed that CMTs usually align with maximal tensile stress in organs from wild-type plants grown in the very same conditions[53] (Fig. 5d). Altogether, these results are consistent with a scenario in which CMTs are able to sense tension, and based on in vitro experiments, they may not require additional factors: they could spontaneously align with maximal tensile stress direction.

A black box: how is stress in the wall transferred to CMTs?

Assuming a physical coupling between the cell wall and the microtubules (Box 2), changes in mechanical stress from the wall could in principle be transferred to microtubules. This is not straightforward. Most plant cells grow perpendicular to the most recent layer of cellulose microfibrils, meaning that if CMTs are aligned with maximal tensile stress, they are also aligned perpendicular to maximal strain. How can CMTs discriminate between stress and strain for their alignment? This is by far the most difficult question to address here. In the context of this perspective article, we provide below some speculations, and experimental suggestions. One of the main drawbacks here is that the exact relation between wall assembly and wall extension remains largely unknown[65], with the possible exception of tip-growing cells like pollen tubes[66].

Because CMTs are physically anchored to the plasma membrane, tension in the wall may propagate to the CMTs, only if such tension was borne by homogeneous material in the wall. However, cell walls are mechanically and chemically heterogeneous. Such heterogeneities are likely to be actively maintained during wall synthesis and remodeling. For instance, the addition of matrix material through secretion (see e.g., [67] Fig. 6c) would allow strain to occur in any direction in principle, but the mechanical anisotropy of cellulose microfibrils biases this effect, by constricting growth direction and only allowing wall deformation between microfibrils. Similarly, the wall remodeler expansins do not promote cell growth through microfibril hydrolysis, but are thought instead to promote polymer creep and increase the spacing between microfibrils[68,69]. This provides a picture of the wall with aligned cellulose microfibrils where tensile stress is high and directional on the one hand, and domains where matrix material accumulates and for which the mechanical status is much more uncertain on the other hand (Fig. 6a). Such mechanical heterogeneities in the wall could generate mechanical conflicts in CMTs.

In that scenario, CMTs may align along stretches of cell walls that are rather homogeneous mechanically, i.e., along cellulose microfibrils or between cellulose microfibrils, but not across alternating cellulose microfibrils and matrix domains (Fig. 6a). This could in principle be tested in in vitro gliding assays but would require building a heterogeneous and stretchable PDMS, which may be difficult to accomplish. Azobenzene lipid could be a good alternative, as corresponding membrane domains can be put under tension upon light stimulation[70]. The analysis of CMTs and cellulose microfibrils in the *mor1* mutant may also be revisited, as this mutant was successfully used in the past to uncouple the deposition of new cellulose microfibrils from pre-existing ones[71].

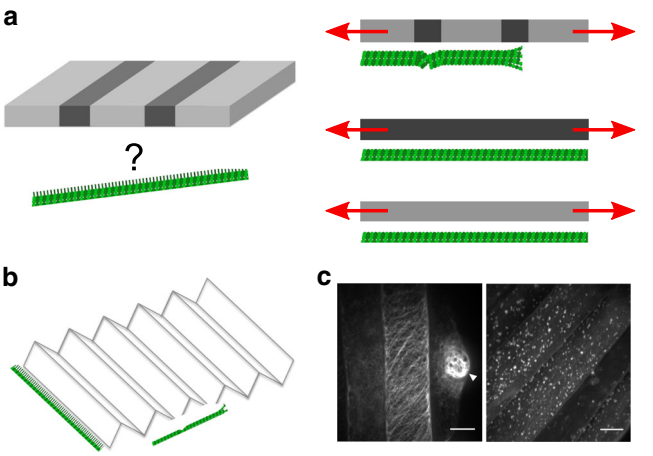

Fig. 6 A role of wall heterogeneities to explain how microtubules distinguish maximal strain from maximal tensile stress. **a** Wall heterogeneities may induce strain discontinuities, destabilizing microtubules, whereas wall homogeneities (e.g., along or between cellulose microfibrils) may stabilize microtubules. **b** Assuming that wall heterogeneities would affect the roughness of the inner face of the wall, the smoother/straighter part of the wall may be parallel to maximal tensile stress direction, along which microtubules (green) would align. **c** Wall heterogeneity may arise from mechanical differences between cellulose microfibrils and the matrix; the delivery of component of the matrix is also heterogeneous in space and time, as shown by click chemistry with alkynylated fucose analogs in roots (left: late differentiation zone, right: early differentiation zone; adapted from ref. [67])

The roughness of the cell wall could also contribute to the nexus between CMT orientation and tensile stress. The inner side of the cell wall is likely to be slightly ruffled, at least at the smallest scales, owing to the heterogeneity of wall components. As the plasma membrane is pushed against the wall in turgid cells, such bumps and valleys may affect the direction of CMT polymerization, (Fig. 6b). Yet, in turgid cells, it is unclear why small ruffles would be aligned with maximal tensile stress. One way to address that question might be to analyze wall shape in the presence of more or less tension. Interestingly, large wall-buckling events can be induced upon strong plasmolysis, and this has even been used to reveal the presence of mechanical conflicts across the wall thickness[72].

Another possible mechanism involves the generation of microcracks as the stress pattern changes. If such abrupt deformations are transferred to the microtubules, they might also destabilize or stabilize them depending on their orientation. Needless to say that the presence of microcracks, the mechanical heterogeneity and roughness of the wall could all contribute to the microtubule response to changes in tensile stress direction.

Last, in addition to wall heterogeneity and shape, it is also possible that the wall integrity pathway[73] has an important role in the relation between CMT orientation and tensile stress in the wall. Interestingly, most sensors have been shown to interact with matrix components so far[74–76]. When cellulose synthesis is artificially inhibited, cell walls can become thicker, an excess of matrix components compensating for the reduction in cellulose microfibrils[77]. This provides a feedback loop for the perception of

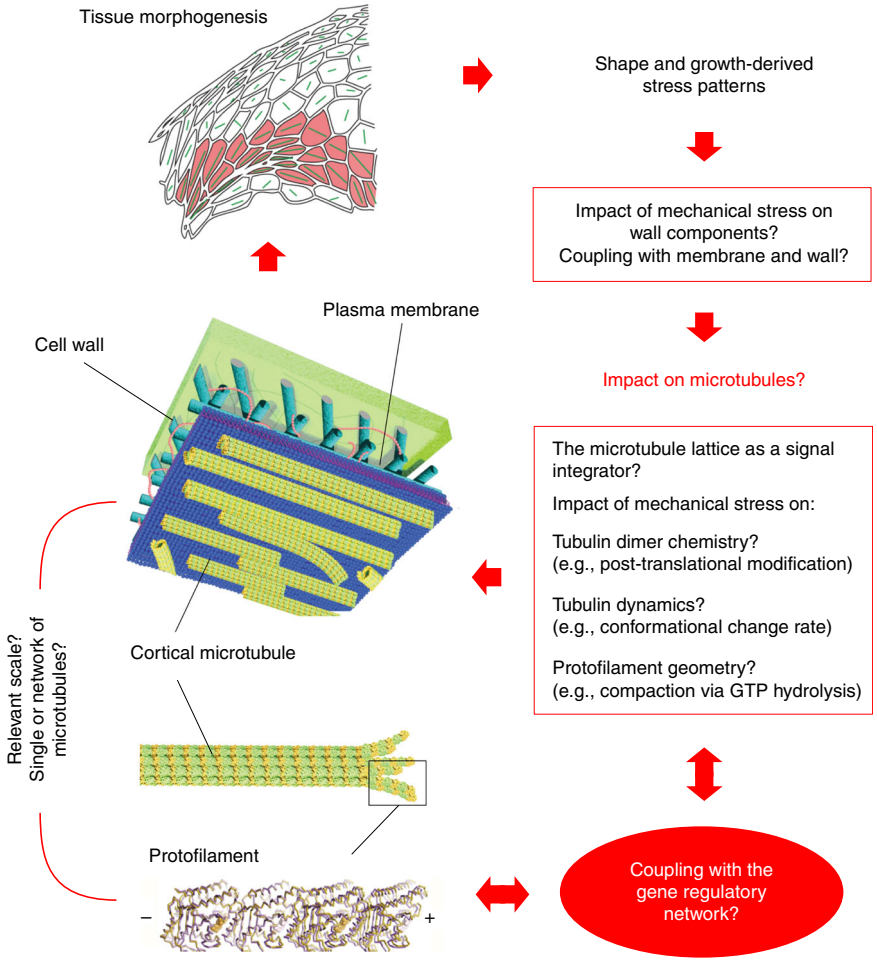

Fig. 7 Integrating the microtubule-tension module in morphogenesis. Plant morphogenesis would emerge from the coupling between inputs from the gene regulatory network and an autonomous microtubule-tension amplifier. In that scenario, the microtubule lattice would be at the crossroad of the biochemical and mechanical control of growth. For instance, GTP hydrolysis within the protofilament leads to the compaction of the tubulin dimer (GTP in orange, GDP in pink—adapted from ref. [46]) and this step may either be modulated by mechanical signals or mimicked by the impact of tension on the protofilament

stress magnitude, not stress direction: wall sensors would trigger the synthesis and delivery of matrix components until they are not pulled by tension anymore. This may indirectly affect CMTs and their relation to stress direction in the wall. For instance, if matrix components are synthesized in excess relative to cellulose microfibrils, this may actively maintain the biochemical and mechanical heterogeneity of the wall. The wall would actively maintain the direction of tension along cellulose microfibrils, because the excess of matrix material would only resist stress magnitude, not stress direction.

These hypotheses are highly speculative and other scenarios could be investigated. Yet, understanding the mechanical and chemical heterogeneity of the wall will likely be instrumental to explain why microtubules in plant cells can change their orientation when maximal tensile stress direction is modified. This is the main missing link behind the hypothesis that microtubules would align along tension on their own in vivo too.

Implications in physiology and development

Our hypothesis raises several questions. First, it is well established that CMTs reorient rapidly in response to many cues, including light[78] or hormones[79]. Similarly, CMTs constantly change their orientations in light-grown hypocotyls[56]. How could this be compatible with a spontaneous CMT response to stress? Although our goal here is not to analyze all scenarios and cues (typically, complex biochemical gradients could also explain supracellular CMTs alignment and their rapid reorientation), the above-mentioned results are not incompatible with the notion that microtubules can function as tension sensors. Indeed, one could expect that blue light rapidly reduces turgor pressure (consistent with the observation that a switch from darkness to light also triggers an immediate reduction in growth rate), and thus tensile stress in the wall: microtubules would switch from their tension-derived orientation (transverse) to their default cell geometry derived orientation (longitudinal, as observed[31]) upon light exposure. Similarly, the constant reorientations of CMTs in light-grown hypocotyls, is not incompatible with the idea that multiple and weak cues (geometry and mechanics) are competing to align CMTs. In fact, it has been proposed that growth direction and local mechanical perturbations compete to orient CMTs in hypocotyls[32].

Second, if our hypothesis is true, we arrive at a mechanical feedback, which requires very little molecular regulation: Upon a change in stress pattern, 1-tubulin dimer in a microtubule lattice would become more stable under tension, 2-Tensed individual CMTs would prevail, biasing the self-organization of CMT arrays in the cell, 3-CMT array alignment along maximal tension would in turn guide cellulose deposition to resist tension and channel the shape of most organs, 4-In turn, organ shape and growth would prescribe the tensile pattern and would maintain CMT orientations (Fig. 7).

Why would plants have selected such a simple mechanism, and what could be its evolutionary significance? Would not this quasi-autonomous mechanical feedback lock cell growth into a dead end, as room for regulation would be reduced to a minimum number of actors? The question of the why is beyond the scope of this article. Yet, it is tempting to propose that the presence of turgor pressure in the MPa range is a strong enough constraint for the cell to have an autonomous mechanism to resist it. If true, an obvious added value of such a self-sustaining CMT-based mechanical feedback would be to offer mechanical resistance by default, enabling fast-growing cell to constantly, rapidly and proportionally adjust to tensile stress in the wall. This could also explain why the relation between tension and microtubules is not as clear in animal cells, where osmotic pressure rather lies in the kPa range.

Last, even in a scenario where CMTs align along maximal tension on their own, the cell still hosts a wide array of potential regulators of the microtubule-tension feedback loop. For instance, the coupling between growth regulation at the cellular level and the microtubule-tension loop could involve modifications within the microtubule lattice. Local defects and post-translational modifications on tubulins could act as a code for molecular regulators to either enhance or reduce the microtubule response to tension (e.g., by modulating their dynamics, their ability to self-repair[28,80], their anchoring to the membrane or their indirect interactions with cellulose microfibrils). For instance, the microtubule-severing enzyme katanin is preferentially recruited at lattice sites exhibiting defects[81], and tubulin acetylation has been shown to mechanically stabilize microtubules[82,83]. The mechanical properties of microtubules are also dependent on bundling factors[84], which likely modify their response to mechanical stress. Another point of coupling lies in the mechanotransduction pathways, which are rather adapted to sense stress intensity and also depend on biochemical signaling (channels, integrins, wall sensors). In fact, we propose here that wall sensors are blind to stress direction, and that this property may be important for CMTs to distinguish between stress and strain: by measuring an excess of tension in the wall, these sensors would promote the synthesis of material in the wall, resulting in a relative deficit of cellulose microfibrils and a relative excess of other components (pectin, hemicellulose), which would maintain a biochemical heterogeneity in the wall, possibly driving CMT orientation independent of cell strain (see Fig. 6).

If microtubules were sensors of tensile stress direction in plants, this would provide a parsimonious scenario in which the robustness of plant shapes would emerge from an autonomous response of microtubules to tension, and where hormones and other cues would regulate this central module either by affecting microtubule dynamics (e.g., with nucleating, bundling or severing factors, or with microtubule anchoring molecules), or by modulating tension levels (e.g., by stiffening or softening the cell walls). In turn, the microtubule response to tension would translate these cues in channeling growth direction, thus amplifying the effect of molecular triggers, locally, while not involving extra molecular control: the microtubule lattice, and its mechanical asymmetry, would be sufficient to provide a directional information for growth. This scenario corresponds to a division of labor between structure and architecture, as initial shape changes would primarily be orchestrated by the gene regulatory network, whereas implementation of shape changes would rely on an autonomous, self-organized, microtubule mechanical feedback (Fig. 7).

Conclusion

Can the role of CMTs as tension sensors be extended to non-cortical microtubules? Kinetochores are interesting case studies for this question, because they couple chromosomes to microtubules, and their dynamics thus provide a force to allow chromosome segregation. The presence of bipolar kinetochores for instance is required for the proper segregation of chromosomes during mitosis (and meiosis II), and the opposing forces exerted by microtubules contribute to such polarity[85]. Conversely, would forces affect the coupling between microtubules and kinetochores? In an elegant experimental set-up, kinetochore–microtubule attachments were reconstituted using purified budding yeast kinetochores, and they were subjected to tensile stress (through cross-linking with beads and displacement with a laser trap). This showed that tension increases the lifetime of such kinetochore–microtubule attachments, notably by affecting several microtubule parameters such as polymerization rate, rescue rate, or catastrophe rate[86]. This is a typical case of catch-bond like association in which dissociation lifetime decreases when tension is applied. Interestingly, such phenomenon occurs at larger scales, such as in cell–cell adhesion: adhesion molecules adhere more tightly in the presence of tension[87], and there is now increasing evidence that such adhesion molecules, like cadherins in animals or pectin in plants, are major players of mechanoperception pathways[88].

Altogether these studies call for a deeper understanding of the links between microtubule biochemistry and mechanics[44]. Therefore, to conclude, here is a list of outstanding questions that remain to be addressed:

1. How does external tension affect the conformation of tubulin dimers and the properties of the microtubule ends and lattice?
2. How does bundling affect the microtubule response to mechanical stress?
3. What are the biochemical and mechanical features of the molecules coupling tension in the wall and cortical microtubules?
4. What are the implications of cell wall heterogeneity on stress propagation to the microtubules?
5. Where and what are the interplays between the molecular regulators of growth and the microtubule response to tension?
6. Does the heterogeneity and defects in the microtubule lattice act as a code for the microtubule response to tension, and thus for the regulation of plant cell growth?
7. What are the larger implications of microtubules aligning with tension, in development and beyond?

Received: 22 October 2018 Accepted: 29 April 2019
Published online: 29 May 2019

References

1. Dalous, J. et al. Reversal of cell polarity and actin-myosin cytoskeleton reorganization under mechanical and chemical stimulation. *Biophys. J.* **94**, 1063–1074 (2008).
2. Théry, M., Jiménez-Dalmaroni, A., Racine, V., Bornens, M. & Jülicher, F. Experimental and theoretical study of mitotic spindle orientation. *Nature* **447**, 493–496 (2007).
3. Engler, A. J., Sen, S., Sweeney, H. L. & Discher, D. E. Matrix elasticity directs stem cell lineage specification. *Cell* **126**, 677–689 (2006).
4. Farge, E. Mechanical induction of Twist in the Drosophila foregut/stomodeal primordium. *Curr. Biol.* **13**, 1365–1377 (2003).
5. Hamant, O. et al. Developmental patterning by mechanical signals in Arabidopsis. *Science* **322**, 1650–1655 (2008).
6. Aigouy, B. et al. Cell flow reorients the axis of planar polarity in the wing epithelium of Drosophila. *Cell* **142**, 773–786 (2010).
7. Pan, Y., Heemskerk, I., Ibar, C., Shraiman, B. I. & Irvine, K. D. Differential growth triggers mechanical feedback that elevates Hippo signaling. *Proc. Natl Acad. Sci. USA* 113, E6974–E6983 (2016).
8. Hervieux, N. et al. A mechanical feedback restricts sepal growth and shape in arabidopsis. *Curr. Biol.* **26**, 1019–1028 (2016).
9. Iskratsch, T., Wolfenson, H. & Sheetz, M. P. Appreciating force and shape—the rise of mechanotransduction in cell biology. *Nat. Rev. Mol. Cell Biol.* **15**, 825–833 (2014).

10. Haswell, E. S., Phillips, R. & Rees, D. C. Mechanosensitive channels: what can they do and how do they do it? *Structure* **19**, 1356–1369 (2011).
11. Yu, M. et al. mDia1 senses both force and torque during F-actin filament polymerization. *Nat. Commun.* **8**, 1650 (2017).
12. Risca, V. I. et al. Actin filament curvature biases branching direction. *Proc. Natl Acad. Sci. USA* **109**, 2913–2918 (2012).
13. Gittes, F., Mickey, B., Nettleton, J. & Howard, J. Flexural rigidity of microtubules and actin filaments measured from thermal fluctuations in shape. *J. Cell Biol.* **120**, 923–934 (1993).
14. Green, P. & King, A. A mechanism for the origin of specifically oriented textures in development with special reference to Nitella wall texture. *Aust. J. Biol. Sci.* **19**, 421–437 (1966).
15. Hejnowicz, Z., Rusin, A. & Rusin, T. Tensile tissue stress affects the orientation of cortical microtubules in the epidermis of sunflower hypocotyl. *J. Plant Growth. Regul.* **19**, 31–44 (2000).
16. Dumont, S. & Mitchison, T. J. Force and length in the mitotic spindle. *Curr. Biol.* **19**, R749–R761 (2009).
17. Green, P. B. Mechanism for plant cellular morphogenesis. *Science* **138**, 1404–1405 (1962).
18. Corson, F. et al. Turning a plant tissue into a living cell froth through isotropic growth. *Proc. Natl Acad. Sci. USA* **106**, 8453–8458 (2009).
19. Elliott, A. & Shaw, S. L. Update: plant cortical microtubule arrays. *Plant Physiol.* **176**, 94–105 (2018).
20. Ehrhardt, D. W. & Shaw, S. L. Microtubule dynamics and organization in the plant cortical array. *Annu. Rev. Plant Biol.* **57**, 859–875 (2006).
21. Moore, R. C., Zhang, M., Cassimeris, L. & Cyr, R. J. In vitro assembled plant microtubules exhibit a high state of dynamic instability. *Cell Motil. Cytoskelet.* **38**, 278–286 (1997).
22. Seltzer, V. et al. Arabidopsis GCP2 and GCP3 are part of a soluble γ-tubulin complex and have nuclear envelope targeting domains: Targeting of γ-tubulin complex proteins. *Plant J.* **52**, 322–331 (2007).
23. Nakamura, M., Lindeboom, J. J., Saltini, M., Mulder, B. M. & Ehrhardt, D. W. SPR2 protects minus ends to promote severing and reorientation of plant cortical microtubule arrays. *J. Cell Biol.* **217**, 915–927 (2018).
24. Dixit, R. & Cyr, R. The cortical microtubule array: from dynamics to organization. *Plant Cell* **16**, 2546–2552 (2004).
25. Wasteneys, G. O. & Ambrose, J. C. Spatial organization of plant cortical microtubules: close encounters of the 2D kind. *Trends Cell Biol.* **19**, 62–71 (2009).
26. Shaw, S. L., Kamyar, R. & Ehrhardt, D. W. Sustained microtubule treadmilling in Arabidopsis cortical arrays. *Science* **300**, 1715–1718 (2003).
27. Chomicki, G., Wightman, R. & Turner, S. R. A specific class of short treadmilling microtubules enhances cortical microtubule alignment. *Mol. Plant* **9**, 1214–1216 (2016).
28. Schaedel, L. et al. Microtubules self-repair in response to mechanical stress. *Nat. Mater.* **14**, 1156–1163 (2015).
29. Fan, Y., Burkart, G. M. & Dixit, R. The arabidopsis SPIRAL2 protein targets and stabilizes microtubule minus ends. *Curr. Biol.* **28**, 987–994.e3 (2018).
30. Uyttewaal, M. et al. Mechanical stress acts via katanin to amplify differences in growth rate between adjacent cells in Arabidopsis. *Cell* **149**, 439–451 (2012).
31. Mirabet, V. et al. The self-organization of plant microtubules inside the cell volume yields their cortical localization, stable alignment, and sensitivity to external cues. *PLoS Comput. Biol.* **14**, e1006011 (2018).
32. Muroyama, A. & Lechler, T. Microtubule organization, dynamics and functions in differentiated cells. *Development* **144**, 3012–3021 (2017).
33. Nakamura, M., Ehrhardt, D. W. & Hashimoto, T. Microtubule and katanin-dependent dynamics of microtubule nucleation complexes in the acentrosomal Arabidopsis cortical array. *Nat. Cell Biol.* **12**, 1064–1070 (2010).
34. Cosentino Lagomarsino, M. et al. Microtubule organization in three-dimensional confined geometries: evaluating the role of elasticity through a combined in vitro and modeling approach. *Biophys. J.* **92**, 1046–1057 (2007).
35. Islam, M. S. et al. Role of confinement in the active self-organization of kinesin-driven microtubules. *Sens. Actuat. B-Chem.* **247**, 53–60 (2017).
36. Ambrose, C., Allard, J. F., Cytrynbaum, E. N. & Wasteneys, G. O. A CLASP-modulated cell edge barrier mechanism drives cell-wide cortical microtubule organization in Arabidopsis. *Nat. Commun.* **2**, 430 (2011).
37. Beer, F. P. & Johnston, E. R. *Mechanics of material*. (McGraw-Hill, 1992).
38. Sampathkumar, A. et al. Subcellular and supracellular mechanical stress prescribes cytoskeleton behavior in Arabidopsis cotyledon pavement cells. *eLife* **3**, e01967 (2014).
39. Sapala, A. et al. Why plants make puzzle cells, and how their shape emerges. *eLife* **7**, e32794 (2018).
40. Kabir, A. M. R. et al. Biomolecular motor modulates mechanical property of microtubule. *Biomacromolecules* **15**, 1797–1805 (2014).
41. Franck, A. D. et al. Tension applied through the Dam1 complex promotes microtubule elongation providing a direct mechanism for length control in mitosis. *Nat. Cell Biol.* **9**, 832–837 (2007).
42. Trushko, A., Schäffer, E. & Howard, J. The growth speed of microtubules with XMAP215-coated beads coupled to their ends is increased by tensile force. *Proc. Natl Acad. Sci. USA* **110**, 14670–14675 (2013).
43. Inoue, D. et al. Sensing surface mechanical deformation using active probes driven by motor proteins. *Nat. Commun.* **7**, 12557 (2016).
44. Brouhard, G. J. & Rice, L. M. Microtubule dynamics: an interplay of biochemistry and mechanics. *Nat. Rev. Mol. Cell Biol.* **19**, 451–463 (2018).
45. Zhang, R., Alushin, G. M., Brown, A. & Nogales, E. Mechanistic origin of microtubule dynamic instability and its modulation by EB proteins. *Cell* **162**, 849–859 (2015).
46. Alushin, G. M. et al. High-resolution microtubule structures reveal the structural transitions in αβ-tubulin upon GTP hydrolysis. *Cell* **157**, 1117–1129 (2014).
47. Sainsbury, F. et al. Developmental reorientation of transverse cortical microtubules to longitudinal directions: a role for actomyosin-based streaming and partial microtubule-membrane detachment. *Plant J.* **56**, 116–131 (2008).
48. Wymer, C. L., Wymer, S. A., Cosgrove, D. J. & Cyr, R. J. Plant cell growth responds to external forces and the response requires intact microtubules. *Plant Physiol.* **110**, 425–430 (1996).
49. Kaverina, I. et al. Tensile stress stimulates microtubule outgrowth in living cells. *J. Cell Sci.* **115**, 2283–2291 (2002).
50. Paredez, A. R., Somerville, C. R. & Ehrhardt, D. W. Visualization of cellulose synthase demonstrates functional association with microtubules. *Science* **312**, 1491–1495 (2006).
51. Jacques, E., Verbelen, J.-P. & Vissenberg, K. Mechanical stress in Arabidopsis leaves orients microtubules in a 'continuous' supracellular pattern. *BMC Plant Biol.* **13**, 163 (2013).
52. Robinson, S. & Kuhlemeier, C. Global compression reorients cortical microtubules in arabidopsis hypocotyl epidermis and promotes growth. *Curr. Biol* **28**, 1794–1802.e2 (2018).
53. Verger, S., Long, Y., Boudaoud, A. & Hamant, O. A tension-adhesion feedback loop in plant epidermis. *eLife* **7**, e34460 (2018).
54. Creff, A., Brocard, L. & Ingram, G. A mechanically sensitive cell layer regulates the physical properties of the Arabidopsis seed coat. *Nat. Commun.* **6**, 6382 (2015).
55. Hardham, A. R., Takemoto, D. & White, R. G. Rapid and dynamic subcellular reorganization following mechanical stimulation of Arabidopsis epidermal cells mimics responses to fungal and oomycete attack. *BMC Plant Biol.* **8**, 63 (2008).
56. Chan, J., Calder, G., Fox, S. & Lloyd, C. Cortical microtubule arrays undergo rotary movements in Arabidopsis hypocotyl epidermal cells. *Nat. Cell Biol.* **9**, 171–175 (2007).
57. Beauzamy, L., Louveaux, M., Hamant, O. & Boudaoud, A. Mechanically, the shoot apical meristem of arabidopsis behaves like a shell inflated by a pressure of about 1 MPa. *Front. Plant Sci.* **6**, 1038 (2015).
58. Burian, A. et al. A correlative microscopy approach relates microtubule behaviour, local organ geometry, and cell growth at the Arabidopsis shoot apical meristem. *J. Exp. Bot.* **64**, 5753–5767 (2013).
59. Heisler, M. G. et al. Alignment between PIN1 polarity and microtubule orientation in the shoot apical meristem reveals a tight coupling between morphogenesis and auxin transport. *PLoS Biol.* **8**, e1000516 (2010).
60. Li, T. et al. Calcium signals are necessary to establish auxin transporter polarity in a plant stem cell niche. *Nat. Commun.* **10**, 726 (2019).
61. Dumais, J. & Steele, C. R. New evidence for the role of mechanical forces in the shoot apical meristem. *J. Plant Growth Regul.* **19**, 7–18 (2000).
62. Kutschera, U. & Niklas, K. J. The epidermal-growth-control theory of stem elongation: an old and a new perspective. *J. Plant Physiol.* **164**, 1395–1409 (2007).
63. Savaldi-Goldstein, S., Peto, C. & Chory, J. The epidermis both drives and restricts plant shoot growth. *Nature* **446**, 199–202 (2007).
64. Vaseva, I. I. et al. The plant hormone ethylene restricts *Arabidopsis* growth via the epidermis. *Proc. Natl Acad. Sci.* **115**, E4130–E4139 (2018).
65. Ali, O. & Traas, J. Force-driven polymerization and turgor-induced wall expansion. *Trends Plant Sci.* **21**, 398–409 (2016).
66. Rojas, E. R., Hotton, S. & Dumais, J. Chemically mediated mechanical expansion of the pollen tube cell wall. *Biophys. J.* **101**, 1844–1853 (2011).
67. Anderson, C. T., Wallace, I. S. & Somerville, C. R. Metabolic click-labeling with a fucose analog reveals pectin delivery, architecture, and dynamics in Arabidopsis cell walls. *Proc. Natl Acad. Sci.* **109**, 1329–1334 (2012).
68. Cosgrove, D. J. Growth of the plant cell wall. *Nat. Rev. Mol. Cell Biol.* **6**, 850–861 (2005).
69. Cosgrove, D. J. Plant cell wall extensibility: connecting plant cell growth with cell wall structure, mechanics, and the action of wall-modifying enzymes. *J. Exp. Bot.* **67**, 463–476 (2016).
70. Hamada, T., Sugimoto, R., Nagasaki, T. & Takagi, M. Photochemical control of membrane raft organization. *Soft Matter* **7**, 220–224 (2011).
71. Himmelspach, R., Williamson, R. E. & Wasteneys, G. O. Cellulose microfibril alignment recovers from DCB-induced disruption despite microtubule disorganization. *Plant J. Cell Mol. Biol.* **36**, 565–575 (2003).

72. Borowska-Wykręt, D. & Kwiatkowska, D. Folding, Wrinkling, and Buckling in Plant Cell Walls. in *Plant Biomechanics* (eds. Geitmann, A. & Gril, J.) 209–233 (Springer International Publishing, 2018).
73. Hématy, K. et al. A receptor-like kinase mediates the response of Arabidopsis cells to the inhibition of cellulose synthesis. *Curr. Biol.* **17**, 922–931 (2007).
74. Wolf, S., Hématy, K. & Höfte, H. Growth control and cell wall signaling in plants. *Annu. Rev. Plant Biol.* **63**, 381–407 (2012).
75. Feng, W. et al. The FERONIA receptor kinase maintains cell-wall integrity during salt stress through Ca2 + signaling. *Curr. Biol* **28**, 666–675.e5 (2018).
76. Kohorn, B. D. The state of cell wall pectin monitored by wall associated kinases: a model. *Plant Signal. Behav.* **10**, e1035854 (2015).
77. Manfield, I. W. et al. Novel cell wall architecture of isoxaben-habituated Arabidopsis suspension-cultured cells: global transcript profiling and cellular analysis. *Plant J. Cell Mol. Biol.* **40**, 260–275 (2004).
78. Lindeboom, J. J. et al. A mechanism for reorientation of cortical microtubule arrays driven by microtubule severing. *Science* **342**, 1245533 (2013).
79. Vineyard, L., Elliott, A., Dhingra, S., Lucas, J. R. & Shaw, S. L. Progressive transverse microtubule array organization in hormone-induced Arabidopsis hypocotyl cells. *Plant Cell* **25**, 662–676 (2013).
80. Aumeier, C. et al. Self-repair promotes microtubule rescue. *Nat. Cell Biol.* **18**, 1054–1064 (2016).
81. Díaz-Valencia, J. D. et al. Drosophila katanin-60 depolymerizes and severs at microtubule defects. *Biophys. J.* **100**, 2440–2449 (2011).
82. Portran, D., Schaedel, L., Xu, Z., Théry, M. & Nachury, M. V. Tubulin acetylation protects long-lived microtubules against mechanical ageing. *Nat. Cell Biol.* **19**, 391–398 (2017).
83. Xu, Z. et al. Microtubules acquire resistance from mechanical breakage through intralumenal acetylation. *Science* **356**, 328–332 (2017).
84. Portran, D. et al. MAP65/Ase1 promote microtubule flexibility. *Mol. Biol. Cell* **24**, 1964–1973 (2013).
85. Nicklas, R. B. The forces that move chromosomes in mitosis. *Annu. Rev. Biophys. Biophys. Chem.* **17**, 431–449 (1988).
86. Akiyoshi, B. et al. Tension directly stabilizes reconstituted kinetochore-microtubule attachments. *Nature* **468**, 576–579 (2010).
87. Dembo, M., Torney, D. C., Saxman, K. & Hammer, D. The reaction-limited kinetics of membrane-to-surface adhesion and detachment. *Proc. R. Soc. Lond. B Biol. Sci.* **234**, 55–83 (1988).
88. Galletti, R., Verger, S., Hamant, O. & Ingram, G. C. Developing a 'thick skin': a paradoxical role for mechanical tension in maintaining epidermal integrity? *Development* **143**, 3249–3258 (2016).
89. Guérin, A., Gravelle, S. & Dumais, J. Forces behind plant cell division. *Proc. Natl Acad. Sci.* **113**, 8891–8893 (2016).
90. Kabir, A. M. R. et al. Buckling of microtubules on a 2D Elastic Medium. *Sci. Rep.* **5**, 17222 (2015).
91. Goldbeter, A. & Koshland, D. E. An amplified sensitivity arising from covalent modification in biological systems. *Proc. Natl Acad. Sci. USA* **78**, 6840–6844 (1981).
92. Liu, Z., Persson, S. & Sánchez-Rodríguez, C. At the border: the plasma membrane-cell wall continuum. *J. Exp. Bot.* **66**, 1553–1563 (2015).
93. Liu, Z., Persson, S. & Zhang, Y. The connection of cytoskeletal network with plasma membrane and the cell wall. *J. Integr. Plant Biol.* **57**, 330–340 (2015).
94. Oda, Y. Emerging roles of cortical microtubule-membrane interactions. *J. Plant Res.* **131**, 5–14 (2018).
95. Martinière, A. et al. Cell wall constrains lateral diffusion of plant plasma-membrane proteins. *Proc. Natl Acad. Sci. USA* **109**, 12805–12810 (2012).
96. Ambrose, J. C. & Wasteneys, G. O. CLASP modulates microtubule-cortex interaction during self-organization of acentrosomal microtubules. *Mol. Biol. Cell* **19**, 4730–4737 (2008).
97. Zhang, Q. & Zhang, W. Regulation of developmental and environmental signaling by interaction between microtubules and membranes in plant cells. *Protein Cell* **7**, 81–88 (2016).
98. Stanislas, T. et al. A phosphoinositide map at the shoot apical meristem in Arabidopsis thaliana. *BMC Biol.* **16**, 20 (2018).
99. Gouget, A. et al. Lectin receptor kinases participate in protein-protein interactions to mediate plasma membrane-cell wall adhesions in Arabidopsis. *Plant Physiol.* **140**, 81–90 (2006).
100. Canut, H. et al. High affinity RGD-binding sites at the plasma membrane of Arabidopsis thaliana links the cell wall. *Plant J. Cell Mol. Biol.* **16**, 63–71 (1998).
101. Bringmann, M. et al. Cracking the elusive alignment hypothesis: the microtubule-cellulose synthase nexus unraveled. *Trends Plant Sci.* **17**, 666–674 (2012).
102. Liu, Z. et al. Cellulose-microtubule uncoupling proteins prevent lateral displacement of microtubules during cellulose synthesis in arabidopsis. *Dev. Cell* **38**, 305–315 (2016).

Acknowledgements

We thank Christophe Godin, Hadrien Oliveri, Jan Traas and Stéphane Verger for comments on this manuscript. This work was supported by Human Frontier Science Program grant RGP0023/2018 and by the European Research Council (ERC-2013-CoG-615739 MechanoDevo).

Author contributions

O.H. drafted the initial article, D.I. wrote the in vitro section of the manuscript (Figs. 2 and 7), E.M. developed a mathematical model of microtubule-tension sensing (Fig. 4), D.B. and J.D. incorporated several important conceptual items to the article. All authors reviewed and contributed to the final version of the article.

Additional information

Competing interests: The authors declare no competing interests.

Reprints and permission information is available online at http://npg.nature.com/reprintsandpermissions/

Journal peer review information: *Nature Communications* thanks Takashi Hashimoto and other anonymous reviewer(s) for their contribution to the peer review of this work.

Publisher's note: Springer Nature remains neutral with regard to jurisdictional claims in published maps and institutional affiliations.

eLIFE elifesciences.org

RESEARCH ARTICLE

A tension-adhesion feedback loop in plant epidermis

Stéphane Verger*, Yuchen Long, Arezki Boudaoud, Olivier Hamant*

Laboratoire de Reproduction et Développement des Plantes, Université de Lyon, ENS de Lyon, UCB Lyon 1, CNRS, INRA, Lyon, France

Abstract Mechanical forces have emerged as coordinating signals for most cell functions. Yet, because forces are invisible, mapping tensile stress patterns in tissues remains a major challenge in all kingdoms. Here we take advantage of the adhesion defects in the *Arabidopsis* mutant *quasimodo1 (qua1)* to deduce stress patterns in tissues. By reducing the water potential and epidermal tension *in planta*, we rescued the adhesion defects in *qua1*, formally associating gaping and tensile stress patterns in the mutant. Using suboptimal water potential conditions, we revealed the relative contributions of shape- and growth-derived stress in prescribing maximal tension directions in aerial tissues. Consistently, the tension patterns deduced from the gaping patterns in *qua1* matched the pattern of cortical microtubules, which are thought to align with maximal tension, in wild-type organs. Conversely, loss of epidermis continuity in the *qua1* mutant hampered supracellular microtubule alignments, revealing that coordination through tensile stress requires cell-cell adhesion.

DOI: https://doi.org/10.7554/eLife.34460.001

***For correspondence:** stephane.verger@ens-lyon.fr (SV); Olivier.Hamant@ens-lyon.fr (OH)

Competing interests: The authors declare that no competing interests exist.

Funding: See page 21

Received: 18 December 2017
Accepted: 20 April 2018
Published: 23 April 2018

Reviewing editor: Dominique C Bergmann, Stanford University/ HHMI, United States

Introduction

As our understanding of the role of forces in development deepens, assessing accurate stress patterns in tissues has become increasingly important (***Roca-Cusachs et al., 2017***). Stress patterns can be revealed through three approaches: 1- Computational models, for example with spring networks or finite elements, with relevant assumptions on tissue mechanics for animal (e.g. [***Sherrard et al., 2010***]) and plant (e.g. [***Bozorg et al., 2014***]) systems, 2- Strain measurements following local cuts at the subcellular (e.g. [***Landsberg et al., 2009***]) or organ (e.g. [***Dumais and Steele, 2000***]) scale, 3- Strain measurement of deformable objects (e.g. FRET-based molecular strain sensors [***Freikamp et al., 2017***], oil microdroplets [***Campàs et al., 2014***], elastomeric force sensors [***Wolfenson et al., 2016***]). Previous work on animal single cells showed that hyperosmotic media can affect membrane tension and thus the molecular effectors of cell migration, like actin filaments, RAC activity or WAVE complex, suggesting that the corresponding mutants could be rescued by a modification of the osmotic conditions of the medium (***Batchelder et al., 2011***; ***Houk et al., 2012***; ***Asnacios and Hamant, 2012***). Consistently, adding sorbitol in growth media is sufficient to rescue defects in yeast endocytic mutants (***Basu et al., 2014***). Here we take inspiration from these single cell studies and apply the same logic at the multicellular scale. Using an *Arabidopsis* mutant with severe cell adhesion defects, we partially rescue these defects by modifying the water potential of the growth medium and we deduce the maximal direction of tension in tissues from the gaping pattern following growth, without any external intervention.

In plants, cell adhesion is achieved through the deposition of a pectin-rich middle lamella between contiguous cell walls (***Orfila et al., 2001***; ***Daher and Braybrook, 2015***; ***Willats et al., 2001***; ***Chebli and Geitmann, 2017***; ***Jarvis et al., 2003***; ***Knox, 1992***). *QUASIMODO1* (*QUA1*) encodes a glycosyltransferase that is required for pectin synthesis and cell adhesion (***Bouton et al., 2002***; ***Mouille et al., 2007***). Here we reasoned that the resulting cell-cell gaps may in principle reveal the

eLife digest The parts of a plant that protrude from the ground are constantly shaken by the wind, applying forces to the plant that it must be able to resist. Indeed, mechanical forces are crucial for the development, growth and life of all organisms and can trigger certain behaviours or the production of particular molecules: for example, forces that bend a plant trigger gene activity that ultimately makes the stem more rigid.

Mechanical forces can also originate from inside the organism. For example, the epidermal cells that cover the surface of a plant are placed under tension by the cells in the underlying layers of the plant as they grow and expand. The exact pattern of forces in the plant epidermis was not known because they cannot be directly seen, although scientists have tried to map them using theoretical and computational modeling.

A mutant form of the *Arabidopsis* plant is unable to produce some of the molecules that allow epidermal cells to adhere to each other. Verger et al. placed the mutants in different growth conditions that lowered the pressure inside the plant, and consequently reduced the tension on the epidermal cells. This partly restored the ability of epidermal cells to adhere to each other, although gaps remained between cells in regions of the plant that have been predicted to be under high levels of tension. Verger et al. could therefore use the patterns of the gaps to map the forces across the epidermis, opening the path for the study of the role of these forces in plant development.

Further experiments showed that cell adhesion defects prevent the epidermal cells from coordinating how they respond to mechanical forces. There is therefore a feedback loop in the plant epidermis: cell-cell connections transmit tension across the epidermis, and, in turn, tension is perceived by the cells to alter the strength of those connections.

The results presented by Verger et al. suggest that plants use tension to monitor the adhesion in the cell layer that forms an interface with the environment. Other organisms may use similar processes; this theory is supported by the fact that sheets of animal cells use proteins that are involved in both cell-cell adhesion and the detection of tension. The next challenge is to analyse how tension in the epidermis affects developmental processes and how a plant responds to its environment.

DOI: https://doi.org/10.7554/eLife.34460.002

stress pattern in tissues. Yet, it has not been formally demonstrated that gap opening could be related to tissue tension. Furthermore, the severe defects in the mutant make it hard to deduce a stress pattern in such distorted tissues. We thus developed a protocol amenable to partially rescue the adhesion defect through water potential modulation, allowing us to relate adhesion to tissue tension on the one hand, and deduce a pattern of stress in various plant tissues on the other hand. This mutant also allowed us to investigate how the loss of adhesion affects the propagation of mechanical stress and thus tension-dependent cell-cell coordination.

Results

Adhesion defects in *qua1* mutants depend on the water potential of the growth medium

The *quasimodo1 (qua1)* and *qua2* mutants, respectively mutated in a galacturonosyltransferase and a pectin methyltransferase, are both required for the synthesis of a fraction of the cell wall pectins. They also display a comparable cell adhesion defect phenotype (***Bouton et al., 2002***; ***Mouille et al., 2007***). For practical reasons, all the work reported in this study was performed with *qua1-1* (WS-4 background), although we observed similar phenotypes in the *qua2-1* mutant (Col-0 background). Because the *qua1* mutant is very sensitive to sucrose in the medium, which leads to metabolic stress and growth arrest of the seedling (***Gao et al., 2008***), we grew the seedlings on a medium containing no sucrose to focus on the cell adhesion phenotype. In these conditions, we could observe cell separation in the epidermis of hypocotyls, stems, cotyledons, and leaves (***Figure 1E***; ***Figure 1—figure supplement 1***), consistent with the epidermal theory of growth where the epidermis is put under

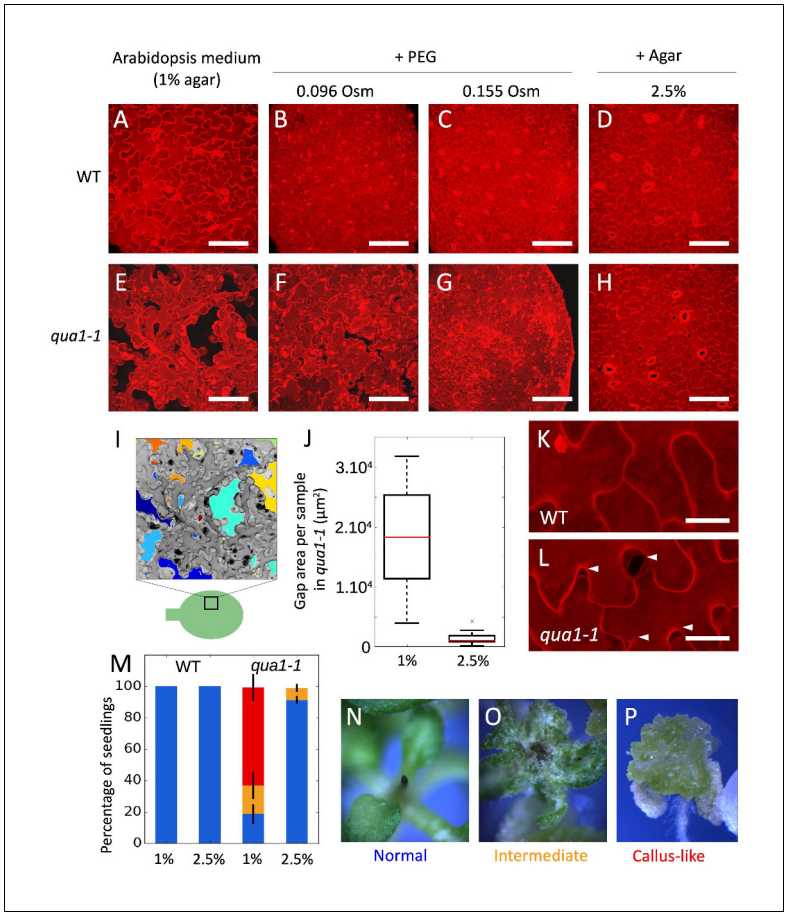

Figure 1. Adhesion defects in *qua1* mutant scale to the water potential of the growth medium. (**A–H**) Z-projections (maximal intensity) of confocal stacks from representative (12 samples observed in three biological replicates for each condition), propidium iodide stained, five days old cotyledons, showing the effect of the decreased medium water potential in the wild type (**A–D**) and the *qua1-1* mutant (**E–H**). A and E are standard growth condition. B-D and F-H are growth conditions with decreased water potential. B, F and C, G water potential is deceased with PEG, which increases the osmolarity of the medium of 96 mOsm (**B, F**) and 155 mOsm (**C, G**). In D and H water potential is decreased by increasing the agar concentration in the medium to 2.5%. (**I**) Representation of the semi automated image analysis process used to detect and quantify the area of gaps per sample shown in I (method further described in the material and method section and ***Figure 1—figure supplement 4***). The upper part: Z-projections (maximal intensity) of a confocal stack in grayscale color and inverted pixel intensity corresponding to panel E. Cell separations are identified and labeled in multiple colors for visualization. The bottom part: schematic representation of a cotyledon and the relative position where Z-stacks were taken (square). (**J**) Box plot of the quantification of the total area of cell separation per image analyzed, in 1% and 2.5% agar growth conditions, and corresponding to the comparison of the panels E and H (12 samples quantified in three biological replicates for each condition, Welch's *t*-test p-value=0.0004). (**K–L**) Close-up from (**D**) and (**H**) respectively, showing the cell separations preferentially happening at the lobe-neck junction (Arrow heads), in the *qua1-1* mutant (**L**). (**M**) Phenotype of the shoot apex in the wild type and *qua1-1* mutant, grown on 1% and 2.5% agar medium (210 seedlings in three biological repetitions per condition, error bars represent the standard deviation over the three biological replicates). Color code is explained in panels N-P: normal stem and meristem (Blue, **N**), a callus-like apex (Red, **P**) or an intermediate phenotype (Orange, **O**). (**N–P**) Stereo microscope images of representative phenotypes as used for the quantifications shown in M. Scale bars (**A–H**), 100 µm. Scale bars (**K,L**), 20 µm.

DOI: https://doi.org/10.7554/eLife.34460.003

The following figure supplements are available for figure 1:

Figure supplement 1. Widespread cell adhesion defects in the *qua1-1* mutant.

DOI: https://doi.org/10.7554/eLife.34460.004

Figure 1 continued on next page

Figure 1 continued

Figure supplement 2. Seedling phenotypes in *qua1* mutant depend on the water potential of the growth medium.

DOI: https://doi.org/10.7554/eLife.34460.005

Figure supplement 3. Dynamics of cell separation in *qua1-1* cotyledon epidermis.

DOI: https://doi.org/10.7554/eLife.34460.006

Figure supplement 4. A semi automated cell separation image analysis pipeline.

DOI: https://doi.org/10.7554/eLife.34460.007

Figure supplement 5. Close-ups of cell-cell adhesion defects in *qua1-1*.

DOI: https://doi.org/10.7554/eLife.34460.008

tension through the pressure exerted by inner tissues, and thus is load-bearing for aerial organs (***Kutschera and Niklas, 2007***; ***Savaldi-Goldstein et al., 2007***; ***Maeda et al., 2014***).

Because endogenous tensile stress in plant epidermis originates both directly and indirectly from turgor pressure, we next modified the water potential of the medium, reasoning that epidermal integrity should be restored in the *qua1* mutant if epidermal tension was decreased.

Increasing concentrations of Polyethylene Glycol (PEG) in the growth medium reduced the growth rate of wild-type and *qua1-1* seedlings, suggesting a reduction in turgor pressure *in planta* caused by a decrease in the water potential of the medium (***Figure 1—figure supplement 2A–C***). Strikingly, in the lowest water potential condition, the overall *qua1-1* phenotype was almost fully rescued (***Figure 1—figure supplement 2E–G***). Using propidium iodide staining and confocal imaging of the cotyledon pavement cells, we further confirmed that such osmotic conditions reduced cell separations in *qua1-1* (***Figure 1E–G***). Note that *qua1-1* pavement cells preferentially separated at the neck-lobe junction, consistent with previously calculated patterns of stress in this tissue (***Figure 1K and L***, [***Sampathkumar et al., 2014***], ***Figure 1—figure supplement 3***, ***Video 1*** and ***2***). This suggests that low tensile stress in the epidermis is sufficient to restore cell adhesion in the mutant.

Nonetheless, because PEG may have pleiotropic effects, we cannot exclude the possibility that the restoration of cell adhesion could be due to other factors. Therefore, we increased agar concentration in the medium, as an alternative way to affect water potential. Indeed,

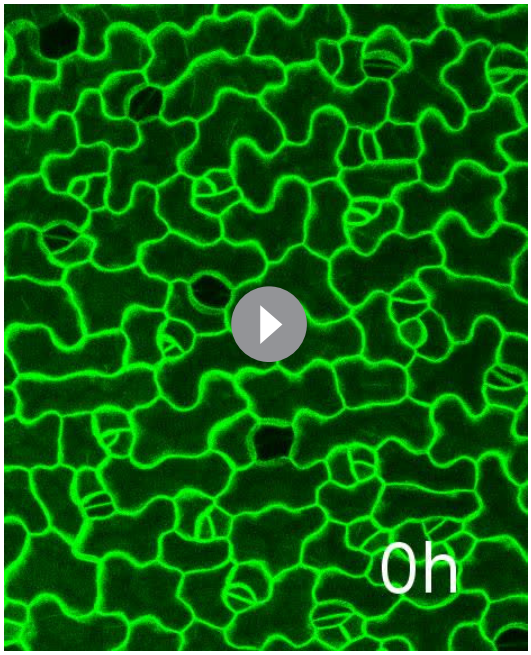

Video 1. Dynamics of cell separation in *qua1-1 pPDF1::mCit:KA1* cotyledon epidermis. Z-projections maximal intensity of confocal stacks taken for 72 hr, at 12 hr intervals.

DOI: https://doi.org/10.7554/eLife.34460.009

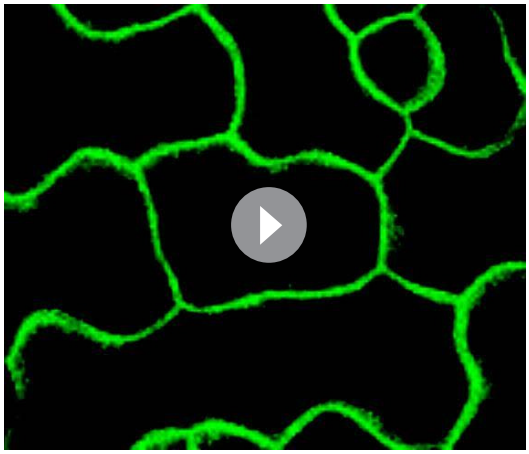

Video 2. Dynamics of cell separation in *qua1-1 pPDF1::mCit:KA1* cotyledon epidermis, high resolution close up of sample 2. Similar to ***Figure 1—figure supplement 3A–D***. Z-projections max intensity of confocal stacks taken for 48 hr, at 12 hr intervals.

DOI: https://doi.org/10.7554/eLife.34460.010

increasing the agar concentration reduces the water potential by decreasing its matrix potential (a component of the water potential, [**Owens and Wozniak, 1991**]) and in turn hinders the capacity of the plant to take up water, as does PEG-containing medium. As expected, we observed a similar restoration of the cell adhesion and seedling phenotype in *qua1-1*, to that observed on PEG-containing medium (**Figure 1H**, **Figure 1—figure supplement 2H**).

To go beyond these qualitative observations, we developed a semi-automated pipeline of image analysis amenable to identify individual gaps between cells, quantify their areas and their main orientations (see Material and methods, **Figure 1I**; **Figure 1—figure supplement 4**; **Verger and Cerutti, 2018**; copy archived at https://github.com/elifesciences-publications/Cell_separation_analysis). Based on images of five-day-old *qua1-1* cotyledons (**Figure 1I**), we found that, for a field of cells representing 138654 μm^2 per image, seedlings grown on 1% agar medium exhibited 17906 (±8955) μm^2 of cell separation per image (i.e. ca. 13% of the surface area, n = 12 samples), while seedlings grown on 2.5% agar medium displayed 1457 (±1140) μm^2 of cell separation per image (i.e. ca. 1% of the surface area, n = 12 samples; **Figure 1J**, Welch's t-test p-value=0.0004), confirming the rescuing effect of a low water potential on cell adhesion.

Last, to confirm that the propidium iodide staining truly reflected cell-cell adhesion defects, we analyzed the gaps in *qua1-1* at different stages with confocal microscopy and, at high resolution, with atomic force microscopy. Our images matched previously published SEM images of *qua1-1* mutants (**Bouton et al., 2002**), with stretched and detached outer walls at the cell-cell junction (**Figure 1—figure supplement 5**). Altogether, these results strongly suggest that adhesion defects in *qua1-1* indeed relate to the tensile status of the tissue.

Adhesion defects in *qua1* mutants specifically relate to epidermal tension

At this stage, we find a correlation between the medium water potential and adhesion defects in *qua1-1*. To measure the impact on epidermal tension, we turned to atomic force microscopy (AFM) to obtain force-displacement curves on epidermal surfaces allowing us to extract a slope, which corresponds to the apparent stiffness of the material (**Figure 2**). We focused on cotyledons, as they are easier to manipulate under the AFM. To maintain tissue hydration, AFM live imaging was conducted in aqueous solutions: for 1% and 2.5% agar-grown cotyledons, cotyledons were submerged in water, while PEG-grown cotyledons were submerged in liquid Arabidopsis medium supplemented with mannitol to reach the same osmotic pressure as the PEG-infused medium (see Materials and methods). To measure cell-level mechanical properties over the epidermal surface, we performed indentations with an AFM probe much smaller than cell size (0.8 µm probe diameter compared to >10 µm cell width; **Figure 2A**). Approximately 10 ~ 15 µN indentations were performed to achieve 1 ~ 2 µm indentation depth (**Figure 2A**), deep enough to detect epidermal turgor pressure but relatively shallow compared to pavement cell thickness (typically 6 ~ 10 µm, [**Zhang et al., 2011**]). In these conditions, we are measuring the stiffness of single epidermal cells, and do not detect the stiffness of the rest of the tissue, notably the internal cell layers (**Beauzamy et al., 2015**).

As shown in **Figure 2**, results obtained from wild-type seedlings grown on medium supplemented with 155 mOsm PEG or 2.5% agar were similar. Similar trends were obtained in *qua1-1*, albeit with a globally reduced turgor pressure, apparent stiffness and cell wall tension (**Figure 2—figure supplement 1**). We also confirmed that the immersion medium had little impact on the measurement both in wild type and *qua1-1*, at least in the short term (**Figure 2—figure supplement 1**). First, we found that turgor pressure levels in the epidermis were not affected by a change in osmotic or matrix potential. This suggests that water potential primarily affect internal tissues and/or that the epidermis can osmoregulate efficiently, as already shown before (e.g. [**Shabala and Lew, 2002**]). Interestingly, when focusing on the outer wall, we found that apparent stiffness decreased by 15% in both PEG and high agar-grown seedlings, while cell wall tension in high agar and PEG-grown seedlings decreased by 18% and 16% respectively, thus demonstrating the impact of the corresponding treatments on epidermal tension. Although such differences in stiffness may appear small, comparable differences were obtained in other tissues, for example between central and peripheral zone of the shoot apical meristem, where differences in growth rates are of 200% to 300% (**Milani et al., 2014**). Furthermore, the concentrations of PEG and agar were chosen so as to maintain growth; in other words, differences could be stronger for higher concentrations, but these would not be relevant for

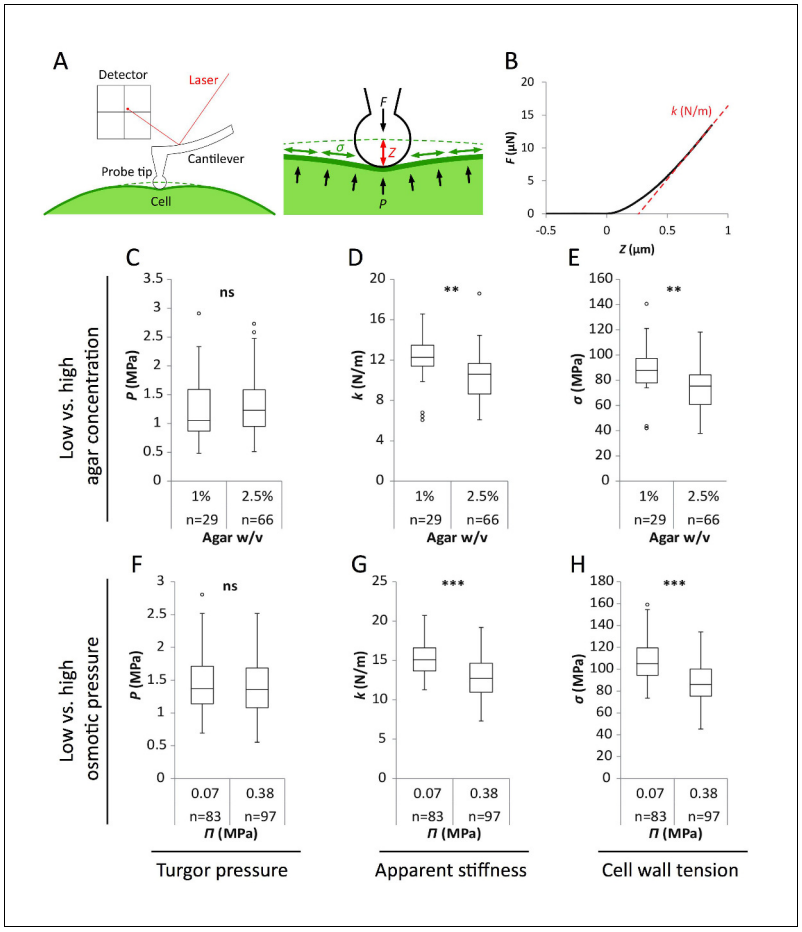

Figure 2. Reduced water potential in growth medium causes decrease in pavement cell stiffness and cell wall tension, not turgor pressure. (**A**) Schematic representation of AFM nano-indentation principle of measurements. *F*, indentation force; *Z*, indentation depth; *P*, turgor pressure; σ, cell wall tension. (**B**) Example of a typical AFM force curve (black line) and linear fit at deep indentation (red dotted line, 75 ~ 99% of maximum force) which depicts apparent stiffness *k*. (**C–H**) Box plots of the turgor pressure *P* (**C**,**F**), apparent stiffness *k* (**D**,**G**) and cell wall tension σ (**E**,**H**) of cotyledon pavement cells grown on medium with differential agar concentration (1% and 2.5% w/v) (**C–E**) or osmotic pressure Π (0.07 and 0.38 MPa) (**F–H**). Circles indicate Tukey's outliers. Student's *t*-test, ** indicates p-value<0.01; ***, p-value<0.001; ns, not significant; *n*, number of measured cells.

DOI: https://doi.org/10.7554/eLife.34460.011

The following figure supplement is available for figure 2:

Figure supplement 1. Controls for AFM measurements.

DOI: https://doi.org/10.7554/eLife.34460.012

our study. Altogether, these data formally relate the decreased water potential in the medium to a decrease in outer wall tension *in planta* and rescue of gaping patterns in *qua1-1*.

Because increasing agar concentration is not toxic to the cell, as shown by propidium iodide staining (see ***Figure 1G and H***), we selected this protocol to alter water potential in the following experiments.

Shape-derived tensile stress dominates at the stem apex

Both shape-derived stress and growth-derived stress contribute to the final pattern of stress in any given field of cells. Shape-derived stress, or pressure stress, is calculated based on the assumption that an organ behaves like a pressure vessel, that is like a load-bearing envelope under tension. This is typically the case for individual plant cells (cell walls resist internal turgor pressure and thus are under tension, see for example (***Sampathkumar et al., 2014***) for an example of stress prediction

entirely based on cell shape) and aerial organs (in the epidermal theory of growth framework, (**Kutschera and Niklas, 2007**), see for example (**Hamant et al., 2008**) for an example of stress prediction entirely based on tissue shape) (**Figure 3N**). Growth-derived stress corresponds to mechanical conflicts arising from differential growth rates or directions ([**Rebocho et al., 2017**; **Thimann and Schneider, 1938**; **Kutschera, 1992**], **Figure 3N**). Using the *qua1-1* mutant, we dissected these two contributions to the global tensile stress patterns in various plant tissues.

First, we analyzed the tensile stress patterns in the inflorescence stem apex, that is where the cells are still actively dividing below the shoot apical meristem (**Figure 3A**). In normal in vitro growth condition, *qua1-1* seedlings often generate aberrant inflorescence meristems and stems, morphologically reminiscent of calli (see **Figure 1P**, and [**Krupková et al., 2007**]). To test whether this phenotype also correlates with the medium water potential, we used *in vitro* grown seedlings to modulate the matrix potential of the growth medium. We also supplemented the medium with NPA, an inhibitor of polar auxin transport and floral organogenesis, to produce naked meristems that are more amenable to visualization and quantification (see e.g. [**Sassi et al., 2014**]). Strikingly, growth on low water potential medium almost completely restored the formation of normal meristems in *qua1-1* with no or only minor loss of cell adhesion (**Figure 3C**, see also **Figure 1M–P**), thereby allowing us to investigate the gaping pattern in *qua1-1* inflorescence stems.

In *qua1-1* plants grown in normal condition (1% agar), we could not distinguish a clear pattern of cell separation, where in most cases the meristem shape was severely affected and some cells seemed to start proliferating randomly (**Figure 3B**). However, when grown on 2.5% agar medium, longitudinal stripes of bright propidium iodide staining were observed in the *qua1-1* mutant stems; such signal could not be detected in the wild type in the same growth conditions (**Figure 3C**). Some of these stripes developed further into cracks between adjacent cells later on, confirming that the stripes correspond to slight separations between adjacent cells where propidium iodide can accumulate, due to the opening of the cuticle at cell junctions and likely unpacking of the cell wall polysaccharides (**Figure 1—figure supplement 5**). In order to quantify these orientations more precisely, we used our cell separation image analysis pipeline, this time focusing on the orientation of cell separation (see **Figure 1—figure supplement 4**). In the stem apex, we obtained a mean gap angle (θ_G) of 91 ± 7° (n = 8 samples), relative to the transverse axis of the stem.

Longitudinal cell separation reveals that the cells are being pulled apart transversely, indicating that maximal epidermal tension is transverse to the axis of the stem. This pattern is consistent with shape-derived stress, assuming that the epidermis acts as a load-bearing layer under tension in that tissue, and thus as in a cylindrical pressure vessel where maximal tension is also transverse (**Figure 3N**).

Note that the age of cell walls may bias our analysis. In particular, based on our results on stem apices, one could propose that older cell walls become less adhesive or more prone to separate. To explore that hypothesis further, we took advantage of our comparative analysis between different tissues to test whether that hypothesis could also hold true.

Growth-derived stress dominates in hypocotyls

While the stem apex grows relatively slowly, hypocotyls grow fast and primarily in one direction, through anisotropic cell expansion (**Gendreau et al., 1997**). In hypocotyls, cell separations happened in several orientations, leading to epidermal cell naturally peeling out of the surface (**Figure 3**; see also **Figure 1—figure supplement 1**). This pattern is thus not consistent with the pressure vessel model in which stress depends only on shape. To explain this discrepancy, we explore the possible contribution of growth-derived stress: the anisotropic expansion of the inner tissues would pull the load-bearing epidermis longitudinally, thus exerting a longitudinal tensile stress on the epidermis (for predictions of longitudinal stress patterns in growing cylindrical organs, see for example [**Baskin and Jensen, 2013**; **Vandiver and Goriely, 2008**]).

To go beyond this qualitative assessment, we next focused on dark-grown hypocotyls, since they display a well characterized gradient of growth during their elongation, in which cells closest to the root (rootward) have already extensively elongated and are undergoing growth arrest, cells more toward the middle are rapidly elongating, and cells at the top (shootward) and in the apical hook are only starting to elongate (**Figure 3—figure supplement 1A**, [**Gendreau et al., 1997**; **Bastien et al., 2016**]). To ensure phenotypic consistency, we observed the rootward part of dark-grown hypocotyls. Because cracks in *qua1* emerge and develop through growth, we reasoned that the gaping pattern

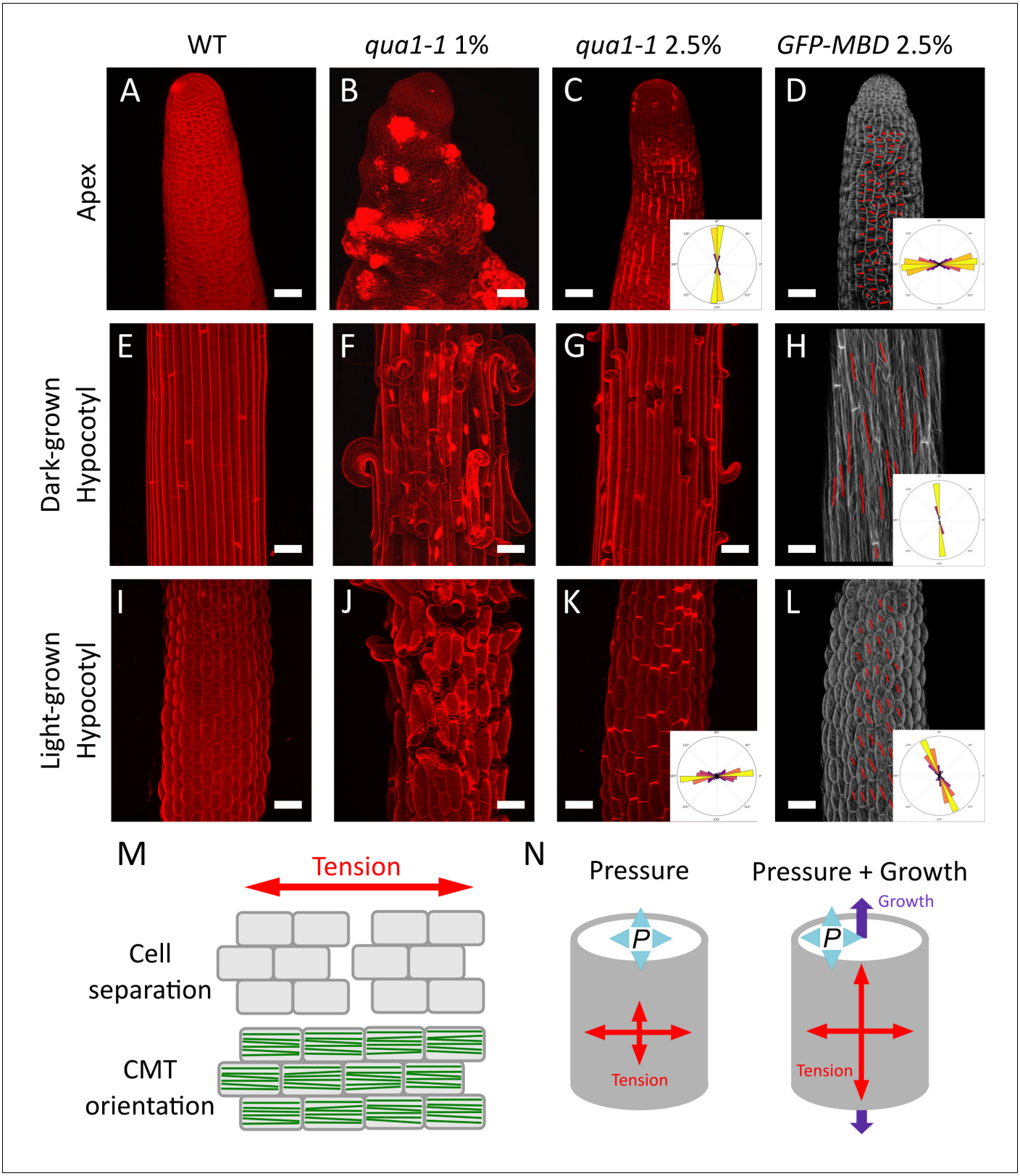

Figure 3. Both shape derived and growth derived tensile stress contribute to the tensile stress pattern in cylindrical organs. (**A–C, E–G and I–K**) Z-projections (maximal intensity) of confocal stacks from representative, propidium iodide stained, shoot apex (**A–C**), dark-grown hypocotyl (**E–G**) and light-grown hypocotyl (**I–K**), from wild type grown on 1% agar medium (**A, E and I**), *qua1-1* grown on 1% agar medium (**B, F and J**) and *qua1-1* grown on 2.5% agar (**C, G and K**). (**D, H and L**) Surface signal extracted from confocal stacks, of representative, *GFP-MBD*, shoot apex (**D**), dark-grown

Figure 3 continued on next page

Figure 3 continued

hypocotyl (**H**) and light-grown hypocotyl (**L**) grown on 2.5% agar medium. Red lines are the output of the FibrilTool macro, giving a visual representation of the cortical microtubule arrays orientation and anisotropy. The polar histograms in C and K show the global distribution of cell separation orientation in 8 samples from three biological replicates. The polar histograms in D, H and L show the distribution of microtubule array orientations for 12 samples. (**M**) Schematic representation of the relationship between tensile stress and cell separation in the *qua1-1* mutant, and cortical microtubule array organization in the wild type. An horizontal tension will pull the cells apart and create a vertical gap between the cells, perpendicular to the tensile stress pattern, while the microtubules in a wild type context will align horizontally, parallel to the tensile stress pattern. (**N**) Schematic representation of the effect of pressure and growth derived stress on the resulting tensile stress pattern in a cylinder. Shape derived stress is caused by the global turgor pressure of the tissue that puts the epidermis under tension. For a cylindrical shape, this results in a tension twice as high in the transverse direction than in the longitudinal direction (***Beer and Johnston, 1992***). Unidirectional growth driven by the inner tissue layers can also put the outer wall of the epidermis under tension, prescribing maximal tensile stress parallel to the growth direction. Scale bars, 50 μm.

DOI: https://doi.org/10.7554/eLife.34460.013

The following figure supplements are available for figure 3:

Figure supplement 1. Dark-grown hypocotyl growth and cell separation patterns.

DOI: https://doi.org/10.7554/eLife.34460.014

Figure supplement 2. Reduction of heterogeneity in pectin esterification in *qua1-1* has no major impact on cell separation patterns.

DOI: https://doi.org/10.7554/eLife.34460.015

Figure supplement 3. CMT behavior in *GFP-MBD* plants grown on 1% agar.

DOI: https://doi.org/10.7554/eLife.34460.016

in this part of the hypocotyl would reflect the stress pattern in cells that previously experienced their maximal elongation phase, *a posteriori* (***Figure 3—figure supplement 1A***). When grown on 1% agar, cell separation patterns were so extensive in dark-grown *qua1-1* hypocotyls that the cell separation patterns could not be quantified properly (***Figure 3F***). When grown on 2.5% agar, we could identify discrete cell separations happening almost exclusively transversely to the axis of dark-grown *qua1-1* hypocotyl (***Figure 3G***). Yet, the presence of cells peeling off suggests that longitudinal cell-cell separation also occurs along the longitudinal axis, likely after the initial transverse separations. Interestingly, this is not consistent with the hypothesis that older cell walls separate first, since all epidermal walls in the hypocotyl have the same age after embryogenesis.

To check whether this pattern depends on mechano-chemical polarities in the anticlinal epidermal cell wall, we next overexpressed *PECTIN METHYLESTERASE INHIBITOR 5* (*PMEI5*) in *qua1-1*, reasoning that *PMEI* overexpression should reduce heterogeneity of pectin esterification in the hypocotyl (***Wolf et al., 2012***; ***Müller et al., 2013***; ***Peaucelle et al., 2015***). Using atomic force microscopy, it was previously shown that wild-type hypocotyls exhibit strong differences in apparent elastic moduli between transverse and longitudinal anticlinal walls in the epidermis, whereas overexpression of *PMEI* significantly reduced such mechanical polarities (***Peaucelle et al., 2015***). As also shown before in *PMEI* overexpressor lines, we observed an increased twisting in the *qua1-1 p35S::PMEI5* line. Yet, we could not detect significant differences in the gaping pattern between dark-grown *qua1-1* and *qua1-1 p35S::PMEI5* hypocotyls, further confirming that the gaping pattern primarily results from the tension pattern (***Figure 3—figure supplement 2***).

The gaps in dark-grown hypocotyls were too large for our image analysis pipeline to precisely discern cell separation orientation (***Figure 3G***). We thus manually counted the number of events of cell separations that happened either at the transverse or longitudinal junction between adjacent cells. In thirteen images from individual hypocotyls, we counted on average about 11 events of cell separation per image. In total, we found 135 events in which cells had separated along their shared transverse wall, and nine events in which they had separated along their shared longitudinal wall. However, among these nine events, seven were related to an adjacent event of transverse cell separation (***Figure 3—figure supplement 1D and E***), while only two events were strictly longitudinal (***Figure 3—figure supplement 1B and C***). Note that cells at the shootward portion of the hypocotyl, where rapid elongation has not started yet, very few cells were separated in *qua1-1* (***Figure 3—figure supplement 1F***), further supporting the role of anisotropic growth in generating the observed gaps.

To further test whether these gaps can indeed be related to growth-derived stress, we took advantage of the ability of hypocotyls to modulate their growth rate according to light conditions: when grown in light, hypocotyls usually reach 1.5 to 2 millimeters in length, in contrast to dark-

grown hypocotyls which can reach about two centimeters (**Gendreau et al., 1997**). We reasoned that, in light conditions, the reduction of elongation should decrease the extent of gap opening in *qua1-1*, while growth anisotropy would still prescribe longitudinal growth-derived stress. As in dark-grown hypocotyls, when grown on 1% agar, cell separation patterns were so extensive in light-grown *qua1-1* hypocotyls that the cell separation patterns could not be quantified properly (**Figure 3J**). When grown on 2.5% agar, transverse gaps were detected in light-grown *qua1-1* hypocotyl (**Figure 3K**). In contrast to dark-grown hypocotyls, we almost only observed slight cell separations in light-grown hypocotyls, as marked by bright propidium iodide staining, consistent with reduced elongation. Because the gaps were much smaller, we could use our pipeline and measured a mean θ_G of 5 ± 30° (**Figure 3K**; **Figure 1—figure supplement 4**, n = 8 samples). A similar response was observed in the *qua1-1 PMEI-OE* line, consistent with the pattern primarily resulting from growth-derived stress, and not from heterogeneities of pectin esterification (**Figure 3—figure supplement 2**).

Altogether, our quantifications support the idea that transverse shape-derived tensile stress dominates in the stem apex epidermis, whereas longitudinal growth-derived stress dominates in the elongating hypocotyl epidermis.

A mechanical conflict at the petiole-blade junction of the cotyledon

Next we investigated the gaping pattern in *qua1-1* cotyledons where more complex shape and growth patterns occur. In comparison to stems and hypocotyls, cotyledon growth occurs mainly in 2D and is rather isotropic (**Zhang et al., 2011**). Using our pipeline, we analyzed cell separation orientation, focusing on cotyledons at a very young stage (3-day old) in order to observe very early cell separations before gaps become too large. No preferential gap orientations could be detected (**Figure 4C**). Note that while an apparent bimodal distribution (with more separations happening at a 0° and 90° angle), the population of angles could be considered uniformly distributed, as assessed using the Rao's spacing test for uniformity (non-parametric test due to the apparent bimodal distribution of the angle population, and adapted for directional data, p-value=0.5, n = 12 samples). This contrasts with the stem apex and the light grown hypocotyl cell separations, for which the test revealed a non-uniform distribution (p-value<0.001 for both). To obtain a different indicator of the spread of the population of angles, we also measured the resultant vector length (R) calculated on these populations of angles. R lies between 0 and 1; the higher it is the more clustered and unidirectional are the data, while a very low value reveals no preferential orientation. R reached 0.84 and 0.70 for the stem apex and light-grown hypocotyls respectively, whereas R was equal to 0.07 for cotyledons. Overall these tests reveal that cell separation and thus tensile stress in the cotyledon epidermis is globally isotropic.

When growing seedlings on a 2.5% agar medium, while almost no more cell separation could be observed on the cotyledon blade (see **Figure 1H and J**), the junction between the petiole and the isotropically expanding cotyledon blade exhibited large cell separations (**Figure 4D and I**). The discrepancy in the extent of cell adhesion defects between blade and junction, as revealed by modulating the water potential, suggests that tensile stress is higher at the blade-petiole junction. When measuring the mechanical properties of the petiole-blade junction with AFM, we actually found that this region exhibits increased turgor pressure, apparent stiffness and surface tension (**Figure 4—figure supplement 1**). Interestingly, using the plasma-membrane-associated protein BREVIS RADIX LIKE 2 (BRXL2) as a polar marker, the proximal region of leaves was recently shown to exhibit increased mechanical stress-driven planar cell polarity (**Bringmann and Bergmann, 2017**). This suggests that the predicted mechanical conflict in the petiole-blade junction of the cotyledon is also present in leaves. To check this, we analyzed the gaping pattern in the third leaf in *qua1-1* and found a pattern roughly similar to that of cotyledons, with longitudinal cracks at the base of the leaf (**Figure 4—figure supplement 2**). Interestingly, in the blade of these leaves, we also observed radial cracks around trichomes, a pattern that is also consistent with the recently identified tensile stress pattern in trichome socket cells (**Hervieux et al., 2017**). Furthermore, gaps at the junction appeared preferentially, but not exclusively, along the longitudinal axis of the petiole (**Figure 4D and I**). Our pipeline revealed that cell adhesion defects displayed a mean θ_G of 85 ± 50° (**Figure 4D and I**, n = 8 samples). Note however that the resultant vector length R was only equal to 0.21 and the Rao's spacing test showed uniformity of the distribution of angles (p-value of 0.5), which suggest that the

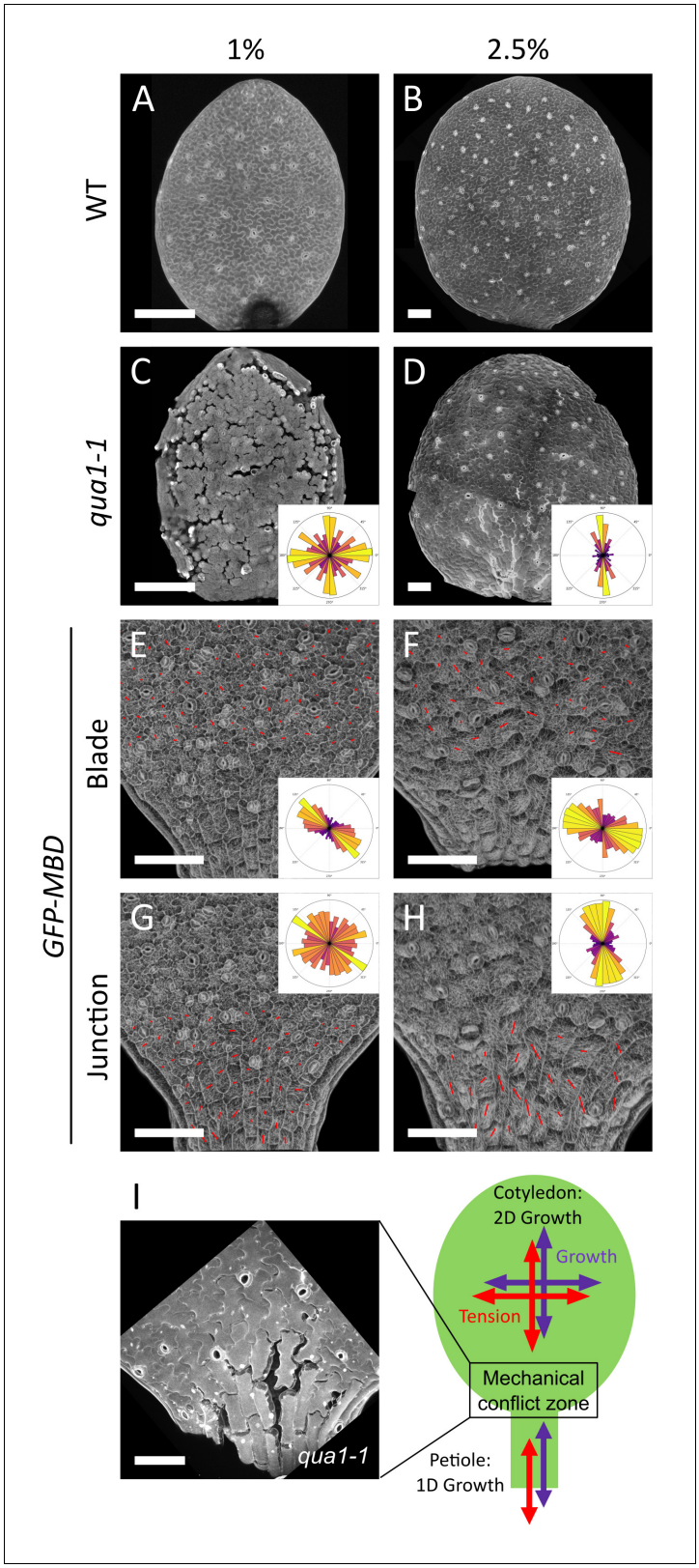

Figure 4. A mechanical conflict at the petiole-blade junction in cotyledons. (**A–D**) Z-projections (maximal intensity) of confocal stacks from representative, propidium iodide stained, 3-day (**A**) or 5-day (**B**) old WT cotyledons and 3-day (**C**) or 5-day (**D**) old *qua1-1* cotyledons grown on 1% (**A, C**) and 2.5% (**B,D**) agar medium. (**E–H**) Surface signal extracted from confocal stacks, of representative *GFP-MBD* cotyledons grown on 1% (E,G; n = 12 cotyledons) and

Figure 4 continued on next page

Figure 4 continued

2.5% (F,H; n = 13 cotyledons) agar medium. Red lines are the output of the FibrilTool macro for the blade region (E (n = 898 cells), F (n = 639 cells)) and petiole-blade junction (G (n = 550 cells), H (n = 425 cells)). The polar histograms in C and D show the global distribution of cell separation orientation in *qua1-1* cotyledons (respectively 12 and 8 samples from three biological replicates); the polar histograms in E-H show the distribution of microtubule array orientations for 12 samples. (**I**) Schematic representation of the effect of differential growth from the cotyledon and the petiole resulting in a mechanical conflict at the junction with higher tensile stress. The close-up image is extracted from a petiole-blade junction in the *qua1-1* mutant. Scale bars, 100 µm.

DOI: https://doi.org/10.7554/eLife.34460.017

The following figure supplements are available for figure 4:

Figure supplement 1. Mechanical assessment of the cotyledon's petiole-blade junction by AFM.

DOI: https://doi.org/10.7554/eLife.34460.018

Figure supplement 2. Gaping pattern in the third leaf of *qua1-1* seedlings.

DOI: https://doi.org/10.7554/eLife.34460.019

bias is weak. Altogether, the analysis of the gaping pattern suggests the presence of a mechanical conflict at the petiole-blade junction in cotyledons, both in intensity and direction (***Figure 4I***).

In the wild type, cortical microtubule orientations match tensile stress patterns, as inferred from cell adhesion defects in *qua1*

To test whether the inferred stress patterns in *qua1-1* are consistent with predicted patterns of stress in the wild type, we next analyzed cortical microtubules (CMTs) in corresponding wild-type organs. CMTs have previously been shown to align along predicted maximal tensile stress direction (***Green and King, 1966***; ***Williamson, 1990***). Such response was observed in sunflower hypocotyl (***Hejnowicz et al., 2000***), *Arabidopsis* shoot apical meristems (***Hamant et al., 2008***), leaves (***Jacques et al., 2013***), cotyledons (***Sampathkumar et al., 2014***) and sepals (***Hervieux et al., 2016***). To check whether tensile stress patterns in aerial organs, as inferred from *qua1-1* cracks, match CMT orientations, we next analyzed the CMT behavior in plants expressing the *p35S::GFP-MBD* microtubule marker (WS-4 ecotype), and quantified the average CMT array orientation (θ_M) and anisotropy using the FibrilTool ImageJ macro (***Figure 5—figure supplement 1***, [***Boudaoud et al., 2014***]).

First, we analyzed CMT orientations in stem apices and cotyledons, where CMT response to mechanical perturbation was already established (***Hamant et al., 2008***; ***Sampathkumar et al., 2014***). CMTs at the stem apex were oriented transversely, matching the stress pattern revealed by the *qua1-1* cell separation patterns (***Figure 3D***; for plants grown on 2.5% agar medium: Mean θ_M = 3 ± 26°, Mean anisotropy = 0.20 ± 0.08, R = 0.65, n = 1669 cells in 13 samples). Note that similar trends were observed on stem apices from seedling grown on 1% and 2.5% agar medium, albeit with a slightly increased noise for seedlings grown on 1% agar medium (***Figure 3—figure supplement 3A,B,E,F***; for plants grown on 1% agar medium: Mean θM = 2 ± 26°, Mean anisotropy = 0.21 ± 0.09, R = 0.66, n = 1604 cells in 12 samples).

CMT exhibited different behaviors between the blade and the petiole-blade junction, consistent with the mechanical conflict revealed by the gaps in *qua1-1* (***Figure 4E–H***). When grown on 1% agar medium, CMTs in the blade exhibited a significant bias in their orientation (Mean θ_M = 150 ± 43°, R = 0.32, n = 898 cells in 12 cotyledons), whereas CMTs at the junction did not exhibit a significant bias in their orientation (R = 0.06, n = 550 cells in 12 cotyledons). Interestingly, the mean anisotropy of the CMT arrays was slightly increased at the junction, when compared to the blade, consistent with the measured increased tension and mechanical conflict in that region (Mean anisotropy = 0.08 ± 0.04 (blade) vs. 0.11 ± 0.06 (junction); paired comparisons between blade and junction from each sample revealed a significant difference (always higher in junction) (Wilcoxon-test, p-values<0.05) for 10 out of 12 samples in each condition). When grown on 2.5% agar medium, the biases in CMT orientation were weak, but significantly different, between the blade and in the junction (blade: mean θ_M = 154 ± 51°, R = 0.19, n = 639 cells in 13 cotyledons; junction: mean θ_M = 97 ± 45°, R = 0.28, n = 425 cells in 13 cotyledons). As on 1% agar medium, the anisotropy of the CMT arrays was higher at the junction (0.18 ± 0.09) than in the blade (0.08 ± 0.05). Paired comparisons between blade and junction from each sample revealed a significant difference (always higher in junction) for 12 out of 13 samples in each condition (Wilcoxon-test, p-values<0.001).

In dark-grown hypocotyls, previous studies had reported that CMTs behave differentially at the inner and outer face of the epidermal cells of the hypocotyl and also display different responses at the hypocotyl shootward region (where cells are not elongated yet), middle (where cell elongation rate is high) and rootward region (where cell elongation is slowing down) (**Chan et al., 2010**; **Chan et al., 2011**; **Crowell et al., 2011**). In particular, CMTs were shown to be transversely oriented in the inner face of the epidermal cell at most of these stages, promoting the anisotropic expansion of the tissue (**Crowell et al., 2011**), whereas CMTs display a puzzling behavior at the outer epidermal face: they are rotating in the top and middle part, and are longitudinal in the bottom part. Focusing on the bottom part of the hypocotyl, where cell separation was observed in *qua1-1*, we observed that CMTs were highly aligned longitudinally in the wild type, when grown in the same conditions as in *qua1-1* (**Figure 3H**; seedlings grown on 2.5% agar medium: Mean θ_M = 98 ± 6°, Mean anisotropy = 0.47 ± 0.06, R = 0.98, n = 182 cells in 12 samples), thus following the tensile stress pattern revealed by the cell separations in *qua1-1*. Note that similar trends were observed for seedling grown on 1% and 2.5% agar medium (**Figure 3—figure supplement 3C,G**; seedling grown on 1% agar medium: Mean θ_M = 93 ± 6°, Mean anisotropy = 0.46 ± 0.04, R = 0.97, n = 137 cells in 10 samples).

In light-grown hypocotyls, CMT orientations seemed random at first sight (see e.g. the scatter plot of CMT orientations in **Figure 5—figure supplement 2D** at t = 0 hr). Consistently, CMTs in light grown-hypocotyl have also been described to harbor a rotating behavior (**Chan et al., 2010**). Yet, when taking into account the anisotropy level of the CMT arrays (to put more weight on CMT orientations when anisotropy is high, as done throughout in this article), we revealed a significant bias towards longitudinal CMT orientations, that is parallel to the tensile stress pattern revealed by the cell separations in *qua1-1* (**Figure 3L**, seedling grown on 2.5% agar medium: Mean θ_M = 113 ± 30°, Mean anisotropy = 0.25 ± 0.10, R = 0.59, n = 606 cells in 11 samples). Note that similar trends were observed for seedling grown on 1% and 2.5% agar medium (**Figure 3—figure supplement 3D,H**; seedling grown on 1% agar medium: Mean θ_M = 109 ± 28°, Mean anisotropy = 0.21 ± 0.08, R = 0.6, n = 413 cells in seven samples). In comparison to dark-grown hypocotyls, the standard deviation was higher, anisotropy and resultant vector length were lower. Note that anisotropy and resultant vector length are describing different properties: anisotropy relates to CMT arrays in individual cells, while vector length relates to the global behavior of CMT arrays in the cell population. Thus lower anisotropy and vector length in light-grown hypocotyls indicates a global reduction of cellular and supracellular CMT alignment. Altogether, these analyses show CMTs globally follow the stress pattern inferred from the cell separations in *qua1-1* (**Figure 3K and L**).

To further explore the relation between mechanical stress and CMT orientation in the hypocotyl, we next analyzed the CMT response to ablation in this tissue. Assuming that the epidermis is under tension, ablations should disrupt pre-established stress pattern and lead to circumferential tensile stress pattern and CMT orientations (**Hamant et al., 2008**; **Sampathkumar et al., 2014**). As expected, reorientation of CMT arrays was observed in hypocotyls 8 hr after ablation, confirming that CMTs can align along maximal tension in hypocotyls too (**Figure 5D and E**). Interestingly, the CMT orientation was however not fully circumferential after ablation. In particular, we sometimes observed radial CMT orientations at the opposite edges along the longitudinal axis of the ablation site, matching the growth-derived longitudinal tensile stress pattern in the hypocotyl (**Figure 5—figure supplement 2A and B**). Conflicts between superposing mechanical stress patterns have been modeled and reported before, notably at the organ-boundary in shoot apical meristems: in that domain, the circumferential CMT orientation after ablation is also mixed, because the boundary is a site of highly anisotropic stresses (see Figure S7 in [**Hamant et al., 2008**]). If such a conflict was not present, one would expect a true circumferential CMT orientation (**Figure 5—figure supplement 2C**). In contrast, our quantifications of the mixed CMT orientations after ablation implies that such a conflict of stress patterns is prominent in hypocotyls (**Figure 5—figure supplement 2D–F**), further consolidating the presence of longitudinal tensile stress in the hypocotyl epidermis.

Overall, CMT orientation and anisotropy correlate well with the tensile stress pattern inferred from the cell separation patterns in *qua1-1*.

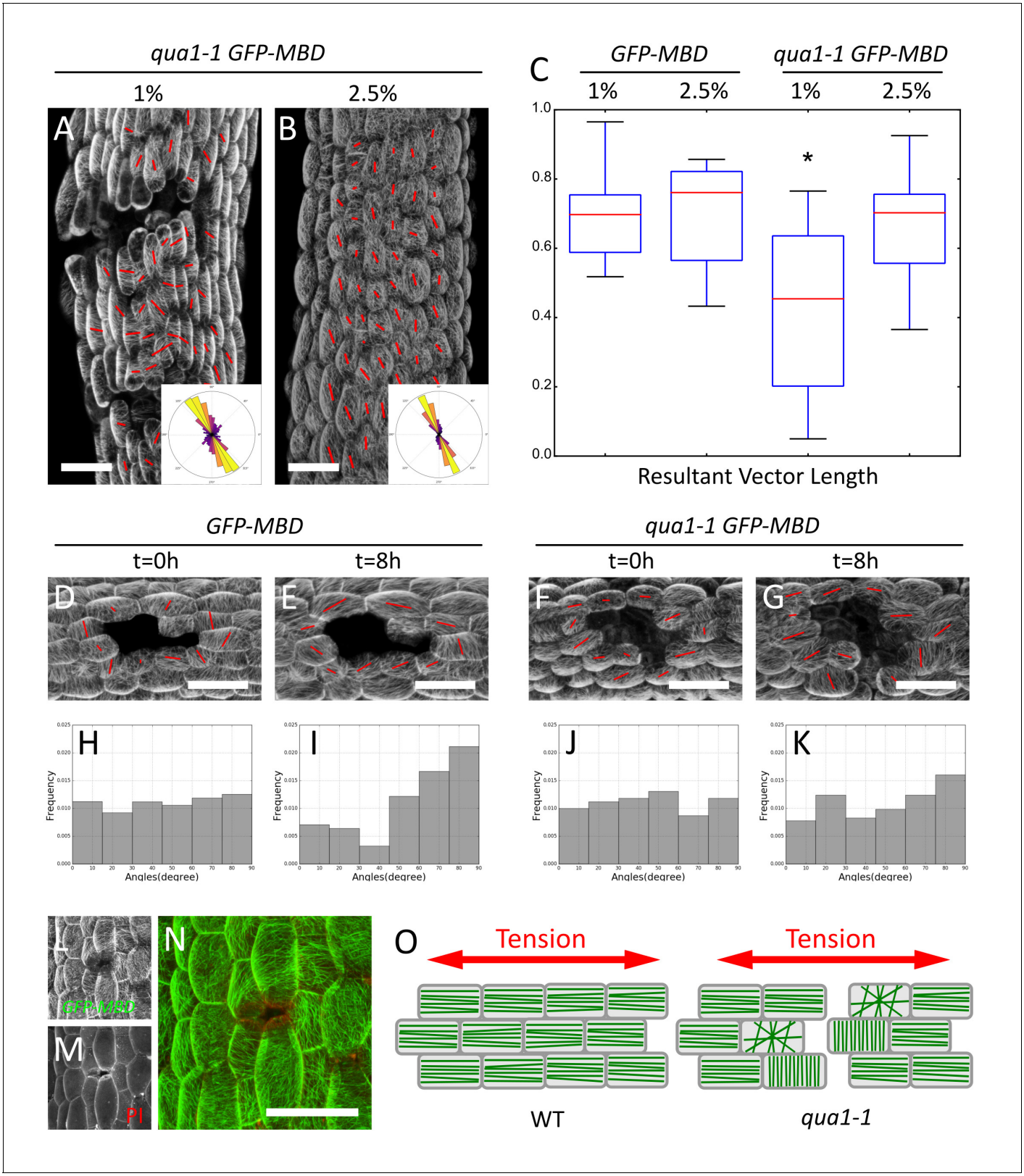

Figure 5. Epidermis continuity is required for tensile stress propagation and supracellular alignment of cortical microtubules. (**A,B**) Surface signal extracted from confocal stacks of representative *qua1-1 GFP-MBD* light-grown hypocotyls. Red lines in A and B are the output of the FibrilTool macro. Cell separation affects cortical microtubule arrays cell to cell coordination across the tissue as compared to ***Figure 3L***. The polar histograms in A and B show the global distribution of microtubule array orientations in 15 (**A**) and 16 (**B**) samples from three biological replicates. (**C**) Box plot of the resultant

Figure 5 continued on next page

Figure 5 continued

vector length revealing less consistent CMT alignment in *qua1-1* hypocotyls grown on 1% agar medium, and a rescue of this defect in *qua1-1* hypocotyls grown on 2.5% agar medium. (**D–K**) Ablation experiment showing the reorganisation of CMT in response to the modified stress pattern in *GFP-MBD* (**D and E**) and *qua1-1 GFP-MBD* (**F and G**), at t = 0 hr after the ablation (**D and F**) and t = 8 hr after the ablation (**E and G**) (10 samples from three biological replicates for each condition). (**H–K**) Histograms of the distributions of CMT array angles relative to the ablation site, and corresponding to panels D-G. (**L–N**) Local impact of a cell-cell adhesion defect in *qua1-1 GFP-MBD*: CMTs align along the local maximum of tension around the gap. (**L**) *GFP-MBD* signal, (**M**) Propidium Iodide signal, (**N**) overlay. (**O**) Schematic representation of the effect of cell separation in the *qua1-1* mutant on cortical microtubule array organization. In the wild type, tension is propagated across the tissue in the epidermis, leading to consistent CMT array alignments in the tissue. In contrast, in *qua1*, the mechanical discontinuity of the epidermis hinders the normal propagation of the tension across the tissue and locally affects the pattern of stress, leading to less pronounced CMT array alignments in the tissue. Scale bars, 50 μm.

DOI: https://doi.org/10.7554/eLife.34460.020

The following figure supplements are available for figure 5:

Figure supplement 1. Surface signal extraction and semi-automated CMT array quantification.

DOI: https://doi.org/10.7554/eLife.34460.021

Figure supplement 2. Conflict between ablation-derived (circumferential) and growth-derived (longitudinal) tensile stress in the hypocotyl outer epidermal cell wall.

DOI: https://doi.org/10.7554/eLife.34460.022

Epidermis continuity is required for tensile stress propagation and the supracellular alignment of cortical microtubules

In plants, the outer epidermal wall is inherited from the zygote and its continuity may be one of the key element to propagate tensile stress over several cell files (***Galletti et al., 2016***). Yet, this still remains to be demonstrated. The analysis of CMTs in *qua1-1* offers us the unique opportunity to test that hypothesis. We thus investigated whether the supracellular microtubule alignment with maximal tensile stress requires an intact outer wall.

We introgressed the *GFP-MBD* microtubule reporter in the *qua1-1* mutant and analyzed microtubule behavior in light-grown hypocotyls, where cracks are mostly superficial early on. Whereas CMTs looked normal within individual *qua1-1* cells, they displayed less consistent orientation at the tissue scale in *qua1-1* cells than in the wild type (***Figures 3L*** and ***5A***). When grown on 1% agar medium, for *GFP-MBD* and *qua1-1 GFP-MBD,* the mean θ_M was 109 ± 28° and 107 ± 40°, the mean anisotropy was 0.21 ± 0.08 and 0.21 ± 0.09 and *R* was 0.6 and 0.36, respectively (*n* = 413 cells in 7 samples and 1019 cells in 16 samples respectively). In other words, the distribution of CMT angles was broader in the *qua1-1* mutant. Note that this discrepancy was also registered when calculating the CMT orientation resultant vector length for each plant individually (allowing us to compare cell populations and test whether the difference is significant): we found a mean resultant vector length for *GFP-MBD* samples of 0.69 ± 0.14 and 0.42 ± 0.23 for *qua1-1 GFP-MBD* and the populations were significantly different (*t*-test p-value=0.012).

Our analysis quantifying the coordination of CMTs across the whole tissue shows that cells in *qua1-1* hypocotyls are less coordinated across the tissue than in the wild type. The presence of cracks may be the main reason for this response: cracks generate local perturbations in the stress pattern, such that CMTs tend to reorganize around these cracks, as shown for cell ablations (***Figure 5L–N*** and e.g. [***Hamant et al., 2008***; ***Hervieux et al., 2016***]). In turn, the actual cell-to-cell coordination does not seem to be affected when two neighboring cells are still attached. Consistently, the anisotropy of CMTs in *qua1-1 GFP-MBD* was not decreased compared to the wild type. In many instances the anisotropy of CMT arrays was higher in *qua1-1 GFP-MBD* and CMTs were somehow oriented following the contours of large gaps, thus apparently following a new tension pattern allowed by the continuity of the cells where they are still adhesive (***Figure 5A,L–N***). Our analysis thus reveals that local cell separations lead to the loss of the tissue-scale organization of the CMTs that is usually found in the wild-type. Therefore, while these data further support a scenario in which epidermis continuity is required for supracellular CMT behavior, the cell-cell separations are too strong to conclude.

When grown on 2.5% agar medium, the wild type and *qua1-1* mutant hypocotyls exhibited similar CMT behaviors: we found a mean resultant vector length for *GFP-MBD* (2.5% agar) samples of 0.69 ± 0.15 and 0.65 ± 0.17 for *qua1-1 GFP-MBD* (2.5% agar) (*n* = 606 cells in 11 samples and 865 cells in 15 samples, respectively) and the populations were not significantly different (*t*-test

p-value=0.556). This is consistent with the phenotypic rescue of the cracks in these conditions, which likely restores the mechanical continuity of the epidermis (**Figure 5B,C**). To test the contribution of epidermis integrity for supracellular CMT orientation along maximal tensile stress, and building on the observed rescue of CMT behavior on 2.5% agar medium, we next modified the mechanical stress pattern in *qua1-1* artificially, using growth conditions in which cracks are only starting to appear. As already shown, cortical microtubule orientation became mostly circumferential in wild type hypocotyls 8 hr after ablation (**Figure 5D and E**). Strikingly, this response was dramatically reduced in *qua1-1* (**Figure 5F and G**). To quantify this response, we calculated the acute angle between the ablation site and the main orientation of the CMT arrays obtained with the FibrilTool macro, for each cell, at t = 0 hr and t = 8 hr after the ablation (**Figure 5—figure supplement 2K**). We thus obtained angles ranging from 0° to 90° (90° corresponding to circumferential CMT orientations around the ablation site, that is parallel to predicted maximal tension). At t = 0 hr, the *GFP-MBD* line exhibited a mean angle of 47 ± 26° showing an homogeneous distribution and no preferred orientation of the microtubules relative to the ablation site (n = 101 cells in 10 samples; **Figure 5H**). At t = 8 hr the mean angle shifted to 58 ± 25°, and the distribution exhibited a strong skewing towards the 80 to 90° angles (n = 101 cells in 10 samples; **Figure 5I**), demonstrating a significant reorganization of the CMT arrays around the ablation site (p-value=0.002). The *qua1-1 GFP-MBD* line however, did not show a significant reorganization of its CMT arrays 8 hr after the ablation (**Figure 5J and K**, Mean angle at t = 0h: 45 ± 26° and t = 8h: 50 ± 26°, n = 107 cells in 10 samples; p-value=0.186). Whereas the distribution of angles still showed a relative skewing towards 90°, the skewness was much smaller than in the *GFP-MBD* line: −0.23 in *qua1-1 GFP-MBD* t = 8 hr vs. −0.77 in *GFP-MBD* t = 8 hr (0,08 in *qua1-1 GFP-MBD* t = 0 hr and −0.04 in *GFP-MBD* t = 0 hr, **Figure 5K**). In addition a statistical test comparing the skewness of the distribution to a corresponding normal distribution showed that the population of angles are not significantly skewed in *GFP-MBD* t = 0 hr, *qua1-1 GFP-MBD* t = 0 hr and *qua1-1 GFP-MBD* t = 8 hr (p-value=0.858, 0.718 and 0.255 respectively), while *GFP-MBD* t = 8 hr shows a significant skewing (p-value=0.002).

Overall, these results demonstrate that a discontinuous outer wall hampers the ability of CMTs to align with supracellular maximal tension in the epidermis (**Figure 5O**).

Discussion

A defining feature of the epidermis in animals is its continuity, which allows a build-up of tension and in turn promotes adhesion and the coordinated behavior of epidermal cells, notably through local cadherin-based cell-cell adhesion (**Galletti et al., 2016**). This loop can be referred as the 'tension-adhesion feedback loop'. The conclusions from the present study support this picture in plants too, notably as tension patterns could be revealed by the early cell-cell adhesion defects in *qua1-1* and as adhesion defects in *qua1-1* hinder the propagation of tensile stress (**Figure 6**).

The physics of pressure vessel, and more generally of solid mechanics, has been instrumental in the derivation of stress patterns in plants, very much in the spirit of D'Arcy Thompson's legacy (**Thompson, 1917**). Yet, the role of mechanical stress in cell and developmental biology remains a subject of heated debate, notably because forces are invisible and stress patterns can only be predicted. Here we used the simplest possible tool to reveal stress pattern in plants, building on cell adhesion defects and their relation to tension. Our results formally validate several conclusions from previous computational models and stress patterns deduced from ablation experiments. Incidentally, this work also brings further experimental proof of the presence of tissue tension, building on the initial work by Hofmeister (**Hofmeister, 1859**) and Sachs (**Sachs, 1878**). We believe this work can serve as a reference for further studies on cell behavior in the corresponding tissues, notably to relate the behavior of cell effectors to stress patterns. Based on these data, one can also revisit previously published work on microtubule behavior in various organs. For instance, it had been reported that CMTs constantly rotate in young hypocotyl until they reach either their transverse or longitudinal orientation (**Chan et al., 2007**). Although this behavior is still an intriguing phenomenon, it could partly be related to the fact that in this tissue, (transverse) shape-derived and (longitudinal) growth-derived stresses are in competition. Slight oscillations in growth rate (**Bastien et al., 2016**) could periodically affect the ratio of shape- and growth-derived stress and thus trigger this rotating behavior of the microtubules. Another exciting avenue for the future is the analysis of the integration between such

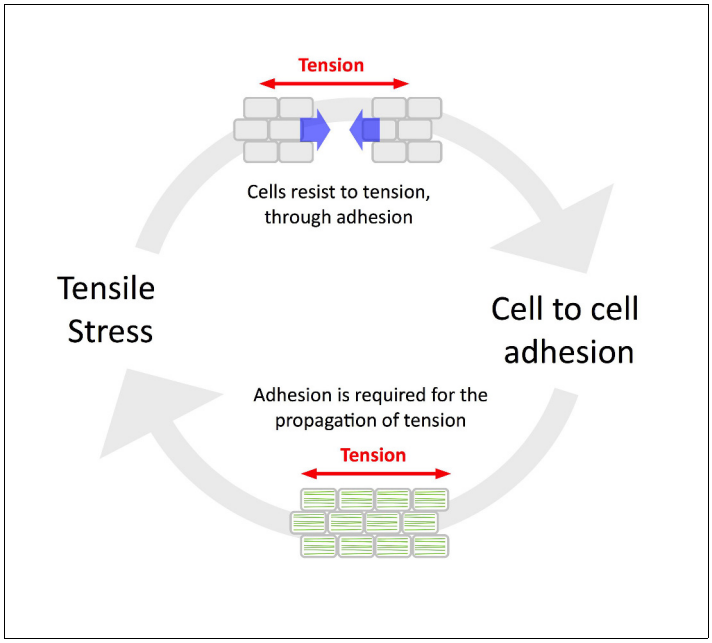

Figure 6. The tension-adhesion feedback loop in plant epidermis. Schematic representation of the relationship between tensile stress and cell to cell adhesion in the epidermis. Tensile stress pulls the cells apart in the *qua1* mutant, while cell to cell adhesion is required to allow the normal propagation of tensile stress in the epidermis, as revealed by the organization of CMT arrays in the *qua1* mutants and the wild type. This paradoxical relationship highlights the importance of epidermis continuity for mechanoperception at the tissue scale.

DOI: https://doi.org/10.7554/eLife.34460.023

tensile stress patterns and other cues such as blue light, and its effect through phototropin and katanin (***Lindeboom et al., 2013***), or hormones (***Vineyard et al., 2013***) on microtubule reorientation.

By definition, mechanical forces can be propagated at the speed of sound, like acoustic waves. This may provide close to instantaneous coordinating cues to tissues, as proposed in the Drosophila wing disc where cell division stops synchronously (***Shraiman, 2005***). Such a mechanism, in turn requires a tightly maintained and controlled cell-to-cell adhesion (***Verger et al., 2016***) in order to constantly maintain the mechanical conductivity of the tissue. Yet, the heterogeneous nature of the tissue would add noise to the signal propagation, and so far this question has not been formally addressed in developmental biology. Here we provide evidence that the continuity of the outer cell wall is required for the coordinated response of adjacent cells to mechanical stress. In other words, a cell would experience different tension level and orientation between a situation where it would be separated from its neighbors (typically, cell shape would be sufficient to prescribe a tensile stress pattern, as in [***Sampathkumar et al., 2014***]) and a situation where it would still adhere to its neighbors (tensile stress could build up at the outer epidermal wall, to a magnitude higher than cell shape-derived stress, and with a pattern that would depend on tissue shape and differential growth, as in [***Hamant et al., 2008***; ***Louveaux et al., 2016***]). This opens exciting prospect for the future, as cell variability and growth heterogeneity is attracting increasing attention because of its, sometimes counterintuitive, instructive function in development (***Hong et al., 2018***).

Note that although CMT alignments match maximal tensile stress direction, as predicted from adhesion defects in *qua1*, this does not necessarily mean that microtubule, and cellulose, become aligned to promote cell-cell adhesion. In fact, mutants in microtubule dynamics or cellulose deposition have not been reported to exhibit adhesion defects. It is therefore more likely that other factors, and most likely actin through its impact on pectin delivery to cell walls (***Mathur et al., 2003***), plays a critical role in the tension-induced reinforcement of cell-cell adhesion, in parallel to microtubule-driven cell wall reinforcement.

Our conclusions also echo the recent analysis of the DEFECTIVE KERNEL 1 (DEK1) protein, which was shown to be required for tensile stress perception *via* its association with a mechanosensitive

Ca^{2+} channel (**Tran et al., 2017**). Interestingly, *DEK1* RNA interference lines exhibit loss of cell adhesion in their epidermis (**Johnson et al., 2005**). Our finding in *qua1* thus allows us to revisit these results, suggesting that plant epidermis requires tensile stress perception, and in turn, that cell-cell adhesion allows tensile stress propagation.

While the coordinating role of the outer wall is difficult to match with a comparable structure in animals, the basement membrane may in principle have a similar role, given its continuity and key role in both adhesion and mechanotransduction. Based on our results in plants, the analysis of basement membrane continuity, and its disruption, may very well help understand how consistent supracellular epidermal patterns relate to mechanical stress, in parallel to the well-established role of cadherin and stress in cell-cell adhesion and epidermal functions (**Galletti et al., 2016**).

Materials and methods

Plant material, genotyping and growth conditions

The *qua1-1* (WS-4) T-DNA insertion line, the *GFP-MBD* (WS-4) microtubule reporter line the *p35S::PMEI5* (Col-0) and the *pPDF1::mCit:KA1* (Col-0) L1 expressed plasma membrane marker, were previously reported in (**Bouton et al., 2002**; **Marc et al., 1998**; **Wolf et al., 2012**; **Simon et al., 2016**) respectively. The *qua1-1* line was genotyped by PCR using the primers described in (**Bouton et al., 2002**) and the *p35S::PMEI5* homozygous lines were selected based on their strong phenotype (**Wolf et al., 2012**; **Müller et al., 2013**).

Arabidopsis thaliana seeds were cold treated for 48 hr to synchronize germination. Plants were then grown in a phytotron at 20°C, in a 16 hr light/8 hr dark cycle on solid custom-made Duchefa 'Arabidopsis' medium (DU0742.0025, Duchefa Biochemie). Seedling age was counted from the start of light exposure.

For dark-grown etiolated hypocotyls, seeds were exposed to light for 4 hr to induce germination. The plates were then wrapped in three layers of aluminum foil to ensure skotomorphogenesis. Naked shoot apical meristems were obtained by adding 10 µM of NPA (N-(1-naphthyl) phthalamic acid) in the medium as described in (**Hamant et al., 2014**).

For time-lapse images of cell separation dynamics, seedlings were first grown on 'Arabidopsis' medium containing 2.5% agar; once cotyledons just opened, they were mounted on 'Arabidopsis' medium containing 1% agar and imaged for up to 72 hr every 12 hr. During image acquisition, the seedlings were immersed in water supplemented with 1 ml of PPM (PPM-Plant Preservative Mixture, Kalys) per liter of medium to prevent contamination. After each acquisition the water was removed and the plants were placed back in a phytotron (see growth conditions above).

Low water potential treatments

Water potential of the medium was changed using either higher agar concentration ((1% and 2.5%) [**Owens and Wozniak, 1991**]) or increasing Polyethylene Glycol. We used a PEG-infused plates method adapted from (**van der Weele et al., 2000**). Classic 1% agar 'Arabidopsis' medium (as described above), as well as liquid 'Arabidopsis' medium containing various concentrations of PEG (PEG20000, Sigma-Aldrich) were prepared. The liquid medium was supplemented with 1 ml of PPM (PPM-Plant Preservative Mixture, Kalys) per liter of medium to prevent contamination. The liquid medium osmolarity was measured using a cryoscopic osmometer (Osmomat 030, Gonotec). Solid medium petri dishes were made, let to solidify for about 2 hr, and an equal volume of liquid medium was poored on top. After 24 hr of diffusion, the liquid medium was recovered and its osmolarity was measured again. The increase of osmolarity due to PEG diffusion in the solid medium was deduced from the difference of osmolarity of the liquid medium before and after diffusion. The petri dishes were let to dry for about 2 hr and the seeds were sown.

Cell wall staining, ablations, confocal microscopy and stereomicroscopy

For cell wall staining, plants were immersed in 0.2 mg/ml propidium iodide (PI, Sigma-Aldrich) for 10 min and washed with water prior to imaging. Ablations were performed as previously described in **Uyttewaal et al., 2012**: seedlings were mounted horizontally with 2% low melting agarose (Sigma-Aldrich, St. Louis, MO, USA) on 'Arabidopsis' medium containing 1% agar and imaged immediately after the ablation and 8 hr after the ablation. The ablations were performed manually with a fine

needle (Minutien pin, 0.15 mm rod diameter, 0.02 mm tip width, RS-6083–15, Roboz Surgical Instrument Co.) ablating approximately five epidermal cells and some cells from the inner layers. Because the size of the ablation can vary from one sample to another, ablations were originally performed on a large number of samples and hypocotyls with comparable number of ablated epidermal cells (approx. 5) were further imaged and analyzed. For imaging, samples were either placed on a solid agar medium and immersed in water, or placed between glass slide and coverslip separated by 400 µm spacers to prevent tissue crushing. Images were acquired using a Leica TCS SP8 confocal microscope. PI excitation was performed using a 552 nm solid-state laser and fluorescence was detected at 600–650 nm. GFP excitation was performed using a 488 nm solid-state laser and fluorescence was detected at 495–535 nm. mCitrine excitation was performed using a 514 nm solid-state laser and fluorescence was detected at 520–555 nm. Stacks of 1024 × 1024 pixels optical section were generated with a Z interval of 0.5 µm for *GFP-MBD*, 1 µm for PI or 0.5 µm when *GFP-MBD* and PI were acquired at the same time and 0.25 µm for *mCit:KA1*. Stereomicroscopy images were taken using a leica MZ12 stereo microscope with an axiocam ICc5 Zeiss CCD camera.

Atomic Force Microscopy

AFM determination of apparent stiffness *k* and turgor pressure *P* in cotyledon epidermis was performed as in (***Beauzamy et al., 2015***) with modifications. Specifically, the adaxial surface of 3 day old cotyledons was measured. Dissected cotyledons grown on different agar concentrations were mounted with Patafix (UHU) and subsequently submerged in water for measurement, whereas whole seedlings grown on different PEG concentrations were mounted in 2% low-melting agarose (Sigma-Aldrich) and submerged in liquid Arabidopsis medium (DU0742.0025, Duchefa Biochemie) supplemented with D-Mannitol (Sigma-Aldrich) to reach the same osmotic pressure of PEG-infused solid medium. Mannitol was used to prevent potential interference of the high viscosity of PEG solutions, and each measurement was performed under 20 min to reduce osmolite uptake. For additional AFM measurements (***Figure 2—figure supplement 1*** and ***Figure 4—figure supplement 1***), whole seedlings grown on different agar concentrations were mounted in 2% low melting agarose (Sigma-Aldrich) and immersed in liquid Arabidopsis medium or water depending on the experiment.

A BioScope Catalyst AFM (Bruker) was used for measurement with spherical-tipped AFM cantilevers of 400 nm tip radius and 42 N/m spring constant (SD-SPHERE-NCH-S-10, Nanosensors). For topography, peak force error and DMT modulus images, PeakForce QNM mode of the acquisition software was used, with peak force frequency at 0.25 kHz and peak force set-point at 1 µN for wild-type and 200 nN for *qua1-1* due to their innate difference in stiffness. Larger peak force set-point frequently damaged *qua1-1* sample surface. 128*128 pixels images of 30*30 μm^2 area were recorded at 0.1 Hz scan rate. For Young's modulus, apparent stiffness and turgor pressure measurements, 1 to 2 µm-deep indentations were performed along the topological skeletons of epidermal cells to ensure relative normal contact between the probe and sample surface. At least three indentation positions were chosen for each cell, with each position consecutively indented three times, making at least nine indentation force curves per cell. Cell registration of AFM force curves were performed with the NanoIndentation plugin for ImageJ (https://fiji.sc/) as described in (***Mirabet et al., 2018***).

Parameters for turgor deduction were generated as follows. Cell wall elastic modulus *E* and apparent stiffness *k* were calculated from each force curve following (***Beauzamy et al., 2015***). Cell surface curvature was estimated from AFM topographic images, with the curvature radii fitted to the long and short axes of smaller cells or along and perpendicular to the most prominent topological skeleton of heavily serrated pavement cells. Turgor pressure was further deduced from each force curve (100 iterations) with the simplified hypothesis that the surface periclinal cell walls of leaf epidermis has constant thickness (200 nm), and cell-specific turgor pressure is retrieved by averaging all turgor deductions per cell.

AFM-measured mechanical properties were used to deduce outer cell wall tension in cotyledon epidermis. Cells were considered as spherical thin-walled pressure vessels, with the stress equals to

$$\sigma = \frac{Pr}{2t}$$

where *P* is turgor pressure, *r* is the vessel radius as the inverse of cell surface mean curvature, and *t*

is assumed cell wall thickness. Since t is assumed constant, σ only depends on turgor pressure and surface topography.

Automated detection of cell separations

The procedure to perform the automated detection of cell separations is described in more detail at Bio-protocol (***Verger et al., 2018***). We developed a semi-automated image analysis pipeline in python language in order to detect and analyze cell separations in a tissue (***Verger and Cerutti, 2018***; copy archived at https://github.com/elifesciences-publications/Cell_separation_analysis). Input images are 2D Z-projections from confocal Z-stack. The script works by segmenting cell separation based on a threshold detection method of pixels intensity. In the case of clear gaps between the cells (as in cotyledons) the pixel intensity is much lower. The threshold allows a segmentation of theses gaps with low intensity pixels. In the case of bright stripes appearing between the cells (as in stem apices or light-grown hypocotyls), an opposite threshold is used, segmenting only the high intensity pixels zones. Because this threshold may vary from one image to the other, it was manually defined using the ImageJ threshold tool before running the script. Running the script then, labels the different zones, measures their areas, performs a principal component analysis of the label in order to determine their main orientations (principal component, θ_G) and assigns an anisotropy and principal angle to each labeled region. The output of the script is an image of every cell separation segmented with a visual representation of their anisotropy, and a polar histogram giving a visual representation of the global result. The python script was developed and run in the TissueLab environment of the OpenAleaLab platform ([***Cerutti et al., 2017***], github.com/VirtualPlants/tissuelab) and using functions from the python libraries SciPy (www.scipy.org), NumPy (www.numpy.org), Pandas (pandas.pydata.org) and Matplotlib (matplotlib.org, see ***Figure 1—figure supplement 4***).

CMT analysis

Original images were confocal Z-stacks. We used the MorphoGraphX software (***Barbier de Reuille et al., 2015***) to recover only the outer epidermal cortical microtubules signal. Further analysis was performed in 2D using the imageJ morpholibJ library (***Legland et al., 2016***), to segment cells, the analyze particle tool to define ROIs and an automated version the FibrilTool macro (***Boudaoud et al., 2014***) to analyze the principal orientation (θ_M) and anisotropy of the CMT arrays (see ***Figure 5—figure supplement 1***).

For the CMT response to ablation, only the cells directly surrounding the ablation were analyzed. Points were manually placed and used to calculate the acute angle between the ablation site and the orientation of the microtubule array for each cell (see ***Figure 5—figure supplement 1***).

Statistical analysis

For linear data (comparing gap area, anisotropy), classical statistical tests were used. Normality of the samples was tested using Shapiro's test. If at least one of the sample population did not have a normal distribution, the populations were compared with the non parametric Wilcoxon Rank Sum test. If both samples had normal distributions, their variance were compared using Bartlett's test. If they were equal, a Student's *t*-test was performed; if they were unequal, a Welch's *t*-test was performed.

For circular (or directional) data (cell separation orientation and CMT orientation), different statistics were used. Since in our case a 0° angle is equal to an 180° angle within a semicircle, the mean, standard deviation, variance, and the accompanied statistical test have to take this fact into account and circular statistics were used. Most of our sample did not show a Von Mises distribution (equivalent of the normal distribution), thus only non-parametric tests were used. The Rao's spacing test was used to determine if the populations of angles were homogeneously distributed, or had a preferred orientation determined by the circular mean.

Finally the data form the CMT response to ablation were treated as linear data, since the calculated angle was between 0° and 90°. The symmetry of CMT response distribution was measured by the skewness of the population towards 90° and the significance of the skewness was tested against a normal distribution.

All statistical analyses were performed in python using the scipy.stats library (scipy.org) for linear data and the pycircstat library (github.com/circstat/pycircstat) for circular data.

Acknowledgements

We thank G Cerutti for help and advices in the design of the cell separation image analysis pipeline, M Liu for technical help, M Dumond for help and advice with statistical analysis. We are thankful to Gwyneth Ingram and Jan Traas for their comments and feedback on this manuscript. This work was supported by the European Research Council (ERC-2013-CoG-615739 'MechanoDevo' and ERC-2012-StG-307387 'Phymorph') and the European Molecular Biology Organization (EMBO ALTF 168–2015).

Additional information

Funding

Funder	Grant reference number	Author
H2020 European Research Council	ERC-2013-CoG-615739	Olivier Hamant
European Molecular Biology Organization	EMBO ALTF 168-2015	Yuchen Long
H2020 European Research Council	ERC-2012-StG-307387	Arezki Boudaoud

The funders had no role in study design, data collection and interpretation, or the decision to submit the work for publication.

Author contributions

Stéphane Verger, Conceptualization, Data curation, Formal analysis, Investigation, Visualization, Methodology, Writing—original draft, Writing—review and editing; Yuchen Long, Data curation, Formal analysis, Investigation, Methodology, Writing—review and editing; Arezki Boudaoud, Supervision, Writing—review and editing; Olivier Hamant, Conceptualization, Supervision, Funding acquisition, Writing—original draft, Project administration, Writing—review and editing

Author ORCIDs

Stéphane Verger https://orcid.org/0000-0003-3643-3978
Olivier Hamant http://orcid.org/0000-0001-6906-6620

Decision letter and Author response

Decision letter https://doi.org/10.7554/eLife.34460.026
Author response https://doi.org/10.7554/eLife.34460.027

Additional files

Supplementary files

- Transparent reporting form

DOI: https://doi.org/10.7554/eLife.34460.024

All data generated or analysed during this study are included in the manuscript and supporting files. Source data file for cell_separation_analysis pipeline has been provided and a reference to Github (where the code is now stored) has been added in the main text and Materials and methods.

References

Asnacios A, Hamant O. 2012. The mechanics behind cell polarity. *Trends in Cell Biology* **22**:584–591. DOI: https://doi.org/10.1016/j.tcb.2012.08.005, PMID: 22980034

Barbier de Reuille P, Routier-Kierzkowska AL, Kierzkowski D, Bassel GW, Schüpbach T, Tauriello G, Bajpai N, Strauss S, Weber A, Kiss A, Burian A, Hofhuis H, Sapala A, Lipowczan M, Heimlicher MB, Robinson S, Bayer EM, Basler K, Koumoutsakos P, Roeder AH, et al. 2015. MorphoGraphX: A platform for quantifying morphogenesis in 4D. *eLife* **4**:05864. DOI: https://doi.org/10.7554/eLife.05864, PMID: 25946108

Baskin TI, Jensen OE. 2013. On the role of stress anisotropy in the growth of stems. *Journal of Experimental Botany* **64**:4697–4707. DOI: https://doi.org/10.1093/jxb/ert176, PMID: 23913952

Bastien R, Legland D, Martin M, Fregosi L, Peaucelle A, Douady S, Moulia B, Höfte H. 2016. KymoRod: a method for automated kinematic analysis of rod-shaped plant organs. *The Plant Journal* **88**:468–475. DOI: https://doi.org/10.1111/tpj.13255, PMID: 27354251

Basu R, Munteanu EL, Chang F. 2014. Role of turgor pressure in endocytosis in fission yeast. *Molecular Biology of the Cell* **25**:679–687. DOI: https://doi.org/10.1091/mbc.E13-10-0618, PMID: 24403609

Batchelder EL, Hollopeter G, Campillo C, Mezanges X, Jorgensen EM, Nassoy P, Sens P, Plastino J. 2011. Membrane tension regulates motility by controlling lamellipodium organization. *PNAS* **108**:11429–11434. DOI: https://doi.org/10.1073/pnas.1010481108, PMID: 21709265

Beauzamy L, Derr J, Boudaoud A. 2015. Quantifying hydrostatic pressure in plant cells by using indentation with an atomic force microscope. *Biophysical Journal* **108**:2448–2456. DOI: https://doi.org/10.1016/j.bpj.2015.03.035, PMID: 25992723

Beer FP, Johnston ER. 1992. *Mechanics of Material*. 2nd edition. McGraw-Hill.

Boudaoud A, Burian A, Borowska-Wykręt D, Uyttewaal M, Wrzalik R, Kwiatkowska D, Hamant O. 2014. FibrilTool, an ImageJ plug-in to quantify fibrillar structures in raw microscopy images. *Nature Protocols* **9**:457–463. DOI: https://doi.org/10.1038/nprot.2014.024, PMID: 24481272

Bouton S, Leboeuf E, Mouille G, Leydecker MT, Talbotec J, Granier F, Lahaye M, Höfte H, Truong HN. 2002. QUASIMODO1 encodes a putative membrane-bound glycosyltransferase required for normal pectin synthesis and cell adhesion in Arabidopsis. *The Plant Cell Online* **14**:2577–2590. DOI: https://doi.org/10.1105/tpc.004259, PMID: 12368506

Bozorg B, Krupinski P, Jönsson H. 2014. Stress and strain provide positional and directional cues in development. *PLoS Computational Biology* **10**:e1003410. DOI: https://doi.org/10.1371/journal.pcbi.1003410, PMID: 24415926

Bringmann M, Bergmann DC. 2017. Tissue-wide mechanical forces influence the polarity of stomatal stem cells in arabidopsis. *Current Biology* **27**:877–883. DOI: https://doi.org/10.1016/j.cub.2017.01.059, PMID: 28285992

Campàs O, Mammoto T, Hasso S, Sperling RA, O'Connell D, Bischof AG, Maas R, Weitz DA, Mahadevan L, Ingber DE. 2014. Quantifying cell-generated mechanical forces within living embryonic tissues. *Nature Methods* **11**:183–189. DOI: https://doi.org/10.1038/nmeth.2761, PMID: 24317254

Cerutti G, Ali O, Godin C. 2017. DRACO-STEM: an automatic tool to generate high-quality 3d meshes of shoot apical meristem tissue at cell resolution. *Frontiers in Plant Science* **8**:353. DOI: https://doi.org/10.3389/fpls.2017.00353, PMID: 28424704

Chan J, Calder G, Fox S, Lloyd C. 2007. Cortical microtubule arrays undergo rotary movements in Arabidopsis hypocotyl epidermal cells. *Nature Cell Biology* **9**:171–175. DOI: https://doi.org/10.1038/ncb1533, PMID: 17220881

Chan J, Crowell E, Eder M, Calder G, Bunnewell S, Findlay K, Vernhettes S, Höfte H, Lloyd C. 2010. The rotation of cellulose synthase trajectories is microtubule dependent and influences the texture of epidermal cell walls in Arabidopsis hypocotyls. *Journal of Cell Science* **123**:3490–3495. DOI: https://doi.org/10.1242/jcs.074641, PMID: 20876662

Chan J, Eder M, Crowell EF, Hampson J, Calder G, Lloyd C. 2011. Microtubules and CESA tracks at the inner epidermal wall align independently of those on the outer wall of light-grown Arabidopsis hypocotyls. *Journal of Cell Science* **124**:1088–1094. DOI: https://doi.org/10.1242/jcs.086702, PMID: 21363888

Chebli Y, Geitmann A. 2017. Cellular growth in plants requires regulation of cell wall biochemistry. *Current Opinion in Cell Biology* **44**:28–35. DOI: https://doi.org/10.1016/j.ceb.2017.01.002, PMID: 28131101

Crowell EF, Timpano H, Desprez T, Franssen-Verheijen T, Emons AM, Höfte H, Vernhettes S. 2011. Differential regulation of cellulose orientation at the inner and outer face of epidermal cells in the Arabidopsis hypocotyl. *The Plant Cell* **23**:2592–2605. DOI: https://doi.org/10.1105/tpc.111.087338, PMID: 21742992

Daher FB, Braybrook SA. 2015. How to let go: pectin and plant cell adhesion. *Frontiers in Plant Science* **6**:523. DOI: https://doi.org/10.3389/fpls.2015.00523, PMID: 26236321

Dumais J, Steele CR. 2000. New evidence for the role of mechanical forces in the shoot apical meristem. *Journal of Plant Growth Regulation* **19**:7–18. DOI: https://doi.org/10.1007/s003440000003, PMID: 11010988

Freikamp A, Mehlich A, Klingner C, Grashoff C. 2017. Investigating piconewton forces in cells by FRET-based molecular force microscopy. *Journal of Structural Biology* **197**:37–42. DOI: https://doi.org/10.1016/j.jsb.2016.03.011, PMID: 26980477

Galletti R, Verger S, Hamant O, Ingram GC. 2016. Developing a 'thick skin': a paradoxical role for mechanical tension in maintaining epidermal integrity? *Development* **143**:3249–3258. DOI: https://doi.org/10.1242/dev.132837

Gao P, Xin Z, Zheng ZL. 2008. The OSU1/QUA2/TSD2-encoded putative methyltransferase is a critical modulator of carbon and nitrogen nutrient balance response in Arabidopsis. *PLoS One* **3**:e1387. DOI: https://doi.org/10.1371/journal.pone.0001387, PMID: 18167546

Gendreau E, Traas J, Desnos T, Grandjean O, Caboche M, Höfte H. 1997. Cellular basis of hypocotyl growth in Arabidopsis thaliana. *Plant Physiology* **114**:295–305. DOI: https://doi.org/10.1104/pp.114.1.295, PMID: 9159952

Green PB, King A. 1966. A Mechanism for the origin of specifically oriented textures in development with special reference to nitella wall texture. *Australian Journal of Biological Sciences* **19**:421. DOI: https://doi.org/10.1071/BI9660421

Hamant O, Heisler MG, Jönsson H, Krupinski P, Uyttewaal M, Bokov P, Corson F, Sahlin P, Boudaoud A, Meyerowitz EM, Couder Y, Traas J. 2008. Developmental patterning by mechanical signals in Arabidopsis. *Science* **322**:1650–1655. DOI: https://doi.org/10.1126/science.1165594, PMID: 19074340

Hamant O, Das P, Burian A. 2014. Time-lapse imaging of developing meristems using confocal laser scanning microscope. *Methods in Molecular Biology* **1080**:111–119. DOI: https://doi.org/10.1007/978-1-62703-643-6_9, PMID: 24132423

Hejnowicz Z, Rusin A, Rusin T. 2000. Tensile tissue stress affects the orientation of cortical microtubules in the epidermis of sunflower hypocotyl. *Journal of Plant Growth Regulation* **19**:31–44. DOI: https://doi.org/10.1007/s003440000005, PMID: 11010990

Hervieux N, Dumond M, Sapala A, Routier-Kierzkowska A-L, Kierzkowski D, Roeder AHK, Smith RS, Boudaoud A, Hamant O. 2016. A mechanical feedback restricts sepal growth and shape in arabidopsis. *Current Biology* **26**:1019–1028. DOI: https://doi.org/10.1016/j.cub.2016.03.004

Hervieux N, Tsugawa S, Fruleux A, Dumond M, Routier-Kierzkowska AL, Komatsuzaki T, Boudaoud A, Larkin JC, Smith RS, Li CB, Hamant O. 2017. Mechanical shielding of rapidly growing cells buffers growth heterogeneity and contributes to organ shape reproducibility. *Current Biology* **27**:3468–3479. DOI: https://doi.org/10.1016/j.cub.2017.10.033, PMID: 29129534

Hofmeister W. 1859. Über die beugungen saftreicher pflanzenteile nach erschütterung. *Ber Verh Ges Wiss Leipz* **11**:175–204.

Hong L, Dumond M, Zhu M, Tsugawa S, Li CB, Boudaoud A, Hamant O, Roeder AHK. 2018. Heterogeneity and robustness in plant morphogenesis: from cells to organs. *Annual Review of Plant Biology*. DOI: https://doi.org/10.1146/annurev-arplant-042817-040517, PMID: 29505739

Houk AR, Jilkine A, Mejean CO, Boltyanskiy R, Dufresne ER, Angenent SB, Altschuler SJ, Wu LF, Weiner OD. 2012. Membrane tension maintains cell polarity by confining signals to the leading edge during neutrophil migration. *Cell* **148**:175–188. DOI: https://doi.org/10.1016/j.cell.2011.10.050, PMID: 22265410

Jacques E, Verbelen JP, Vissenberg K. 2013. Mechanical stress in Arabidopsis leaves orients microtubules in a 'continuous' supracellular pattern. *BMC Plant Biology* **13**:163. DOI: https://doi.org/10.1186/1471-2229-13-163, PMID: 24138025

Jarvis MC, Briggs SPH, Knox JP. 2003. Intercellular adhesion and cell separation in plants. *Plant, Cell and Environment* **26**:977–989. DOI: https://doi.org/10.1046/j.1365-3040.2003.01034.x

Johnson KL, Degnan KA, Ross Walker J, Ingram GC. 2005. AtDEK1 is essential for specification of embryonic epidermal cell fate. *The Plant Journal* **44**:114–127. DOI: https://doi.org/10.1111/j.1365-313X.2005.02514.x, PMID: 16167900

Knox JP. 1992. Cell adhesion, cell separation and plant morphogenesis. *The Plant Journal* **2**:137–141. DOI: https://doi.org/10.1111/j.1365-313X.1992.00137.x

Krupková E, Immerzeel P, Pauly M, Schmülling T. 2007. The Tumorous shoot developmenT2 gene of Arabidopsis encoding a putative methyltransferase is required for cell adhesion and co-ordinated plant development. *The Plant Journal* **50**:735–750. DOI: https://doi.org/10.1111/j.1365-313X.2007.03123.x, PMID: 17461780

Kutschera U. 1992. The role of the epidermis in the control of elongation growth in stems and coleoptiles. *Botanica Acta* **105**:246–252. DOI: https://doi.org/10.1111/j.1438-8677.1992.tb00294.x

Kutschera U, Niklas KJ. 2007. The epidermal-growth-control theory of stem elongation: an old and a new perspective. *Journal of Plant Physiology* **164**:1395–1409. DOI: https://doi.org/10.1016/j.jplph.2007.08.002, PMID: 17905474

Landsberg KP, Farhadifar R, Ranft J, Umetsu D, Widmann TJ, Bittig T, Said A, Jülicher F, Dahmann C. 2009. Increased cell bond tension governs cell sorting at the Drosophila anteroposterior compartment boundary. *Current Biology* **19**:1950–1955. DOI: https://doi.org/10.1016/j.cub.2009.10.021, PMID: 19879142

Legland D, Arganda-Carreras I, Andrey P. 2016. MorphoLibJ: integrated library and plugins for mathematical morphology with ImageJ. *Bioinformatics* **32**:3532–3534. DOI: https://doi.org/10.1093/bioinformatics/btw413, PMID: 27412086

Lindeboom JJ, Nakamura M, Hibbel A, Shundyak K, Gutierrez R, Ketelaar T, Emons AM, Mulder BM, Kirik V, Ehrhardt DW. 2013. A mechanism for reorientation of cortical microtubule arrays driven by microtubule severing. *Science* **342**:1245533. DOI: https://doi.org/10.1126/science.1245533, PMID: 24200811

Louveaux M, Julien JD, Mirabet V, Boudaoud A, Hamant O. 2016. Cell division plane orientation based on tensile stress in Arabidopsis thaliana. *PNAS* **113**:E4294–E4303. DOI: https://doi.org/10.1073/pnas.1600677113, PMID: 27436908

Maeda S, Gunji S, Hanai K, Hirano T, Kazama Y, Ohbayashi I, Abe T, Sawa S, Tsukaya H, Ferjani A. 2014. The conflict between cell proliferation and expansion primarily affects stem organogenesis in Arabidopsis. *Plant and Cell Physiology* **55**:1994–2007. DOI: https://doi.org/10.1093/pcp/pcu131, PMID: 25246492

Marc J, Granger CL, Brincat J, Fisher DD, Kao T, McCubbin AG, Cyr RJ. 1998. A GFP-MAP4 reporter gene for visualizing cortical microtubule rearrangements in living epidermal cells. *The Plant Cell* **10**:1927–1940. DOI: https://doi.org/10.2307/3870914, PMID: 9811799

Mathur J, Mathur N, Kernebeck B, Hülskamp M. 2003. Mutations in actin-related proteins 2 and 3 affect cell shape development in Arabidopsis. *The Plant Cell Online* **15**:1632–1645. DOI: https://doi.org/10.1105/tpc.011676, PMID: 12837952

Milani P, Mirabet V, Cellier C, Rozier F, Hamant O, Das P, Boudaoud A. 2014. Matching patterns of gene expression to mechanical stiffness at cell resolution through quantitative tandem epifluorescence and nanoindentation. *Plant Physiology* **165**:1399–1408. DOI: https://doi.org/10.1104/pp.114.237115, PMID: 24924426

Mirabet V, Krupinski P, Hamant O, Meyerowitz EM, Jönsson H, Boudaoud A. 2018. The self-organization of plant microtubules inside the cell volume yields their cortical localization, stable alignment, and sensitivity to external cues. *PLOS Computational Biology* **14**:e1006011. DOI: https://doi.org/10.1371/journal.pcbi.1006011, PMID: 29462151

Mouille G, Ralet MC, Cavelier C, Eland C, Effroy D, Hématy K, McCartney L, Truong HN, Gaudon V, Thibault JF, Marchant A, Höfte H. 2007. Homogalacturonan synthesis in Arabidopsis thaliana requires a Golgi-localized protein with a putative methyltransferase domain. *The Plant Journal* **50**:605–614. DOI: https://doi.org/10.1111/j.1365-313X.2007.03086.x, PMID: 17425712

Müller K, Levesque-Tremblay G, Bartels S, Weitbrecht K, Wormit A, Usadel B, Haughn G, Kermode AR. 2013. Demethylesterification of cell wall pectins in Arabidopsis plays a role in seed germination. *Plant Physiology* **161**:305–316. DOI: https://doi.org/10.1104/pp.112.205724, PMID: 23129203

Orfila C, Seymour GB, Willats WG, Huxham IM, Jarvis MC, Dover CJ, Thompson AJ, Knox JP. 2001. Altered middle lamella homogalacturonan and disrupted deposition of (1–>5)-alpha-L-arabinan in the pericarp of Cnr, a ripening mutant of tomato. *Plant Physiology* **126**:210–221. DOI: https://doi.org/10.1104/pp.126.1.210, PMID: 11351084

Owens LD, Wozniak CA. 1991. Measurement and effects of gel matric potential and expressibility on production of morphogenic callus by cultured sugarbeet leaf discs. *Plant Cell, Tissue and Organ Culture* **26**:127–133. DOI: https://doi.org/10.1007/BF00036116

Peaucelle A, Wightman R, Höfte H. 2015. The control of growth symmetry breaking in the arabidopsis hypocotyl. *Current Biology* **25**:1746–1752. DOI: https://doi.org/10.1016/j.cub.2015.05.022, PMID: 26073136

Rebocho AB, Southam P, Kennaway JR, Bangham JA, Coen E. 2017. Generation of shape complexity through tissue conflict resolution. *eLife* **6**:e20156. DOI: https://doi.org/10.7554/eLife.20156, PMID: 28166865

Roca-Cusachs P, Conte V, Trepat X. 2017. Quantifying forces in cell biology. *Nature Cell Biology* **19**:742–751. DOI: https://doi.org/10.1038/ncb3564, PMID: 28628082

Sachs J. 1878. Über die Anordnung der Zellen in jüngsten Pflanzentheilen. *Arb Bot Inst* **2**:46–104.

Sampathkumar A, Krupinski P, Wightman R, Milani P, Berquand A, Boudaoud A, Hamant O, Jönsson H, Meyerowitz EM. 2014. Subcellular and supracellular mechanical stress prescribes cytoskeleton behavior in Arabidopsis cotyledon pavement cells. *eLife* **3**:e01967. DOI: https://doi.org/10.7554/eLife.01967, PMID: 24740969

Sassi M, Ali O, Boudon F, Cloarec G, Abad U, Cellier C, Chen X, Gilles B, Milani P, Friml J, Vernoux T, Godin C, Hamant O, Traas J. 2014. An auxin-mediated shift toward growth isotropy promotes organ formation at the shoot meristem in Arabidopsis. *Current Biology* **24**:2335–2342. DOI: https://doi.org/10.1016/j.cub.2014.08.036, PMID: 25264254

Savaldi-Goldstein S, Peto C, Chory J. 2007. The epidermis both drives and restricts plant shoot growth. *Nature* **446**:199–202. DOI: https://doi.org/10.1038/nature05618, PMID: 17344852

Shabala SN, Lew RR. 2002. Turgor regulation in osmotically stressed Arabidopsis epidermal root cells. Direct support for the role of inorganic ion uptake as revealed by concurrent flux and cell turgor measurements. *Plant Physiology* **129**:290–299. DOI: https://doi.org/10.1104/pp.020005, PMID: 12011359

Sherrard K, Robin F, Lemaire P, Munro E. 2010. Sequential activation of apical and basolateral contractility drives ascidian endoderm invagination. *Current Biology* **20**:1499–1510. DOI: https://doi.org/10.1016/j.cub.2010.06.075, PMID: 20691592

Shraiman BI. 2005. Mechanical feedback as a possible regulator of tissue growth. *PNAS* **102**:3318–3323. DOI: https://doi.org/10.1073/pnas.0404782102, PMID: 15728365

Simon ML, Platre MP, Marquès-Bueno MM, Armengot L, Stanislas T, Bayle V, Caillaud MC, Jaillais Y. 2016. A PtdIns(4)P-driven electrostatic field controls cell membrane identity and signalling in plants. *Nature Plants* **2**:16089. DOI: https://doi.org/10.1038/nplants.2016.89, PMID: 27322096

Steeling C. 1970. Crystal-structure of ruthenium red and stereochemistry of its pectic stain. *American Journal of Botany* **57**:172–175. DOI: https://doi.org/10.1002/j.1537-2197.1970.tb09804.x

Thimann KV, Schneider CL. 1938. Differential growth in plant tissues. *American Journal of Botany* **25**:627–641. DOI: https://doi.org/10.1002/j.1537-2197.1938.tb09271.x

Thompson DW. 1917. *On Growth and Form*. Cambridge, UK: Cambridge University press.

Tran D, Galletti R, Neumann ED, Dubois A, Sharif-Naeini R, Geitmann A, Frachisse JM, Hamant O, Ingram GC. 2017. A mechanosensitive Ca^{2+} channel activity is dependent on the developmental regulator DEK1. *Nature Communications* **8**:1009. DOI: https://doi.org/10.1038/s41467-017-00878-w, PMID: 29044106

Uyttewaal M, Burian A, Alim K, Landrein B, Borowska-Wykręt D, Dedieu A, Peaucelle A, Ludynia M, Traas J, Boudaoud A, Kwiatkowska D, Hamant O. 2012. Mechanical stress acts via katanin to amplify differences in growth rate between adjacent cells in Arabidopsis. *Cell* **149**:439–451. DOI: https://doi.org/10.1016/j.cell.2012.02.048, PMID: 22500806

van der Weele CM, Spollen WG, Sharp RE, Baskin TI. 2000. Growth of arabidopsis thaliana seedlings under water deficit studied by control of water potential in nutrient-agar media. *Journal of Experimental Botany* **51**:1555–1562. DOI: https://doi.org/10.1093/jexbot/51.350.1555, PMID: 11006306

Vandiver R, Goriely A. 2008. Tissue tension and axial growth of cylindrical structures in plants and elastic tissues. *EPL* **84**:58004. DOI: https://doi.org/10.1209/0295-5075/84/58004

Verger S, Chabout S, Gineau E, Mouille G. 2016. Cell adhesion in plants is under the control of putative O-fucosyltransferases. *Development* **143**:2536–2540. DOI: https://doi.org/10.1242/dev.132308, PMID: 27317803

Verger S, Cerutti G, Hamant O. 2018. An image analysis pipeline to quantify emerging cracks in materials or adhesion defects in living tissues. *Bio-Protocol* **8**:e3036. DOI: https://doi.org/10.21769/BioProtoc.3036

Verger S, Cerutti G. 2018. Cell_separation_analysis. *GitHub*. 8fe7334. https://github.com/sverger/Cell_separation_analysis

Vineyard L, Elliott A, Dhingra S, Lucas JR, Shaw SL. 2013. Progressive transverse microtubule array organization in hormone-induced Arabidopsis hypocotyl cells. *The Plant Cell* **25**:662–676. DOI: https://doi.org/10.1105/tpc.112.107326, PMID: 23444330

Willats WG, McCartney L, Mackie W, Knox JP. 2001. Pectin: cell biology and prospects for functional analysis. *Plant Molecular Biology* **47**:9–27. DOI: https://doi.org/10.1023/A:1010662911148, PMID: 11554482

Williamson RE. 1990. Alignment of cortical microtubules by anisotropic wall stresses. *Australian Journal of Plant Physiology* **17**:601–613. DOI: https://doi.org/10.1071/PP9900601

Wolf S, Mravec J, Greiner S, Mouille G, Höfte H. 2012. Plant cell wall homeostasis is mediated by brassinosteroid feedback signaling. *Current Biology* **22**:1732–1737. DOI: https://doi.org/10.1016/j.cub.2012.07.036, PMID: 22885061

Wolfenson H, Meacci G, Liu S, Stachowiak MR, Iskratsch T, Ghassemi S, Roca-Cusachs P, O'Shaughnessy B, Hone J, Sheetz MP. 2016. Tropomyosin controls sarcomere-like contractions for rigidity sensing and suppressing growth on soft matrices. *Nature Cell Biology* **18**:33–42. DOI: https://doi.org/10.1038/ncb3277, PMID: 26619148

Zhang C, Halsey LE, Szymanski DB. 2011. The development and geometry of shape change in Arabidopsis thaliana cotyledon pavement cells. *BMC Plant Biology* **11**:27. DOI: https://doi.org/10.1186/1471-2229-11-27, PMID: 21284861